



**HAL**  
open science

## **Kinetic Study and Model Assessment for n -Butyl Levulinate Production from Alcoholysis of 5-(Hydroxymethyl)furfural over Amberlite IR-120**

Daniele Di Menno Di Bucchianico, Antonella Cipolla, Jean-Christophe Buvat, Mélanie Mignot, Valeria Casson Moreno, Sébastien Leveneur

► **To cite this version:**

Daniele Di Menno Di Bucchianico, Antonella Cipolla, Jean-Christophe Buvat, Mélanie Mignot, Valeria Casson Moreno, et al.. Kinetic Study and Model Assessment for n -Butyl Levulinate Production from Alcoholysis of 5-(Hydroxymethyl)furfural over Amberlite IR-120. Industrial and engineering chemistry research, 2022, 10.1021/acs.iecr.2c01640 . hal-03731262

**HAL Id: hal-03731262**

**<https://normandie-univ.hal.science/hal-03731262>**

Submitted on 20 Jul 2022

**HAL** is a multi-disciplinary open access archive for the deposit and dissemination of scientific research documents, whether they are published or not. The documents may come from teaching and research institutions in France or abroad, or from public or private research centers.

L'archive ouverte pluridisciplinaire **HAL**, est destinée au dépôt et à la diffusion de documents scientifiques de niveau recherche, publiés ou non, émanant des établissements d'enseignement et de recherche français ou étrangers, des laboratoires publics ou privés.

Kinetic study and model assessment for the n-butyl levulinate production from the alcoholysis  
of 5-HMF over Amberlite IR-120

Daniele Di Menno Di Bucchianico<sup>1,2,\*1</sup>, Antonella Cipolla<sup>1,2,\*</sup>, Jean-Christophe Buvat<sup>1</sup>,

Mélanie Mignot<sup>3</sup>, Valeria Casson Moreno<sup>2</sup> and Sébastien Leveneur<sup>1\*</sup>

<sup>1</sup>Normandie Univ, INSA Rouen, UNIROUEN, LSPC, EA4704, 76000 Rouen, France,

[sebastien.leveneur@insa-rouen.fr](mailto:sebastien.leveneur@insa-rouen.fr);

<sup>2</sup>Dipartimento di Ingegneria Chimica, Civile, Ambientale e dei Materiali, Alma Mater

Studiorum—Università di Bologna, via Terracini 28, 40131 Bologna, Italy;

<sup>3</sup>COBRA UMR CNRS 6014, Normandie Université, INSA de Rouen, avenue de l'Université,

Saint-Etienne-du-Rouvray, 76800, France

---

<sup>1\*</sup> These authors contributed equally to the work.

## Abstract

Alkyl levulinates such as n-butyl levulinate (BL) can play an important role in the fuel sector. Classically, BL is produced from the esterification of LA, but the butanolysis (or alcoholysis) of sugars requires less stages. The industrialization of this process requires the development of process flow diagrams and thus, the knowledge of reaction kinetics and thermodynamics. To the best of our knowledge, there are no kinetic models for the production of BL from sugar butanolysis over heterogeneous catalysts. The kinetics of sugar monomer butanolysis is complex over heterogeneous catalysts due to several side-reactions, e.g., esterification and humins productions. Hence, developing a kinetic model strategy is vital by primarily focusing on the butanolysis of 5-HMF over Amberlite IR-120. The butanolysis of 5-(hydroxymethyl)furfural (5-HMF) is the crucial step for the production of BL. The effect of temperature, catalyst and 5-HMF loadings, and catalyst deactivation on the kinetics of the different species were investigated. Then, different kinetic models were developed and tested by cross-validation. Special attention was given to vary widely the reaction temperature, catalyst and 5-HMF loadings. To increase the accuracy of the estimation stage, independent experiments of levulinic and formic acids esterification, side-products of 5-HMF dehydration, were included. It was found that the developed model with more reaction steps and by considering the reaction of humins production from 5-HMF as first-order was the most reliable model.

Keywords: Lignocellulosic biomass, Cellulose valorization, Butyl levulinate production, 5-(hydroxymethyl) furfural) alcoholysis, Amberlite IR-120, Humins production, Kinetic modeling, K-fold method

## 1. Introduction

Fossil raw materials in modern society plays a crucial role. However, using such raw materials has several drawbacks: non-renewable, difficult to extract (i.e., not full extraction), resources are not well-distributed at global scale and negative environmental impacts such as perturbation in the carbon cycle (released of greenhouse gas) or oil spills.

In order to overcome these drawbacks, the shift from fossil non-renewable raw materials to biomass renewable raw materials can aid our modern societies to continue their developments with a minimum impact on the environment. Biomass valorization faces several challenges such as biomass collection network, catalyst development, diversity of biomass content, oxygen and water presence, pretreatment,<sup>1</sup> etc. The use of biomass for chemical production is not new in chemical processes, one can cite the production of alcohol from cereals or sugar juice. Nevertheless, the use of such raw materials competes with food. To avoid the food versus fuel dilemma, agricultural waste or non-alimentary plants should be favored.

Lignocellulosic biomass can avoid such a dilemma and enhance the circular economy.<sup>2-4</sup> Lignocellulosic biomass has a fascinating structure made of lignin (natural aromatic polymer) and cellulose/hemicellulose which are sugar polymers. The composition of these elements is different for each plant, implying that operating conditions should be tuned for each biomass. The first stage is to separate lignin, cellulose and hemicellulose, i.e., the fractionation stage. The valorization of lignin is still under development for industrial application.<sup>5-8</sup> The valorization of cellulose and hemicellulose is more developed,<sup>9-13</sup> notably for the industrial production of cellulosic ethanol.

From the cellulose or hemicellulose valorization, it is possible to develop several platform molecules such as: 1,4-diacid, 5-(hydroxymethyl)furfural (5-HMF), 2,5-furandicarboxylic acid (2,5-FDCA), aspartic acid, glutamic acid, glucaric acid, itaconic acid, sorbitol, acetone-butanol-ethanol (ABE process) or levulinic acid<sup>14-16</sup>. Some of them are already at the industrial scale, such as levulinic acid one.<sup>17,18</sup>

Levulinic acid can be the starting materials for several chemicals (solvents, materials or fuels) like  $\gamma$ -valerolactone<sup>19,20,21</sup>, succinic acid,<sup>22–24</sup> 2-methylene  $\gamma$ -valerolactone<sup>25</sup> or 2-methyltetrahydrofuran (2-MTHF).<sup>26–28</sup> The classical production of LA is from the hydrolysis of cellulose using homogeneous catalysts.<sup>29–32</sup> Nevertheless, the low yields in LA production, together with high costs in separation and purification of this acid, make the direct production of alkyl levulinates more beneficial via sugar alcoholysis<sup>33</sup>.

Among alkyl levulinates, methyl, ethyl and butyl levulinates are the most studied and used in the literature. As shown in the review of Di Menno Di Bucchianico et al.,<sup>33</sup> alcoholysis of sugars over heterogeneous acid catalysts should be favored for the production of alkyl levulinates compared to the traditional homogeneous acids. Zhou et al.,<sup>34</sup> reported the production of methyl levulinate from glucose, catalyzed by aluminum sulfate at 160 °C for 3 h, obtaining a production yield of 64%. Saravanamurugan and Riisager<sup>35</sup> studied the production of ML from fructose over zeolite (H-USY) at 160 °C for 20 h with a final ML yield of 51 %. The production of methyl levulinate was also investigated starting from 5-HMF by Hu et al.,<sup>36</sup> using Amberlyst 70 at 120 °C for 2 h and resulting in a final yield of 61.7 %. Wang et al.,<sup>37</sup> reported the total conversion of 5-HMF and the final yield in ML of 69.6 % over the zeolite H-beta-40. From a green-chemistry aspect, ethyl and butyl levulinates production can be considered greener because ethanol and butanol are produced from renewable raw materials. Ethyl levulinate production has been studied over a wide range of heterogeneous catalysts and starting materials. Liu et al.,<sup>38</sup> have investigated the conversion of fructose over Amberlyst-15 at 120 °C for 24 h, obtaining a final yield of 73 % for ethyl levulinate and 89 % for butyl levulinate. Considering different feedstocks, Quereshi et al.,<sup>39</sup> showed the increase in EL yield passing from glucose (23 %), to fructose (25 %) and to 5-HMF (37.2 %) over a metal salt. 5-HMF alcoholysis in ethanol was also studied on zeolite (MZSM-5) by Chithra and Srinivas<sup>40</sup> with a final EL yield of 85.2 % at 150 °C for 12 h. Studies on the production of butyl levulinate are mainly from sugar alcoholysis, as the investigation of Di Menno Di Bucchianico et al.,<sup>41</sup> on fructose conversion over Amberlite IR120 with a final yield 60.4 % at 110 °C for 7 h or the work

of An et al.,<sup>42</sup> with  $\text{Fe}_2(\text{SO}_4)_3$  reporting a final BL yield of 62.8 % at 190 °C. Fewer literature data are on the production of butyl levulinate, although, from an energy point of view, the use of butyl levulinate as blend in fuels has certain advantages compared to ethyl levulinate in terms of conductivity, cold flow properties, diesel lubrication, reduced vapour pressure, corrosivity and miscibility with fuels even at very low temperatures.<sup>41</sup>

Some kinetic models of sugar hydrolysis to levulinic acid and esterification (levulinic acid to alkyl levulinates and formic acid to alkyl formate) can be found in the literature<sup>29,43–50</sup>. However, the development of kinetic models for the alcoholysis of sugars to alkyl levulinates is scarce, and the kinetic constant comparison is difficult due to the different ways to derive reaction rates.<sup>51</sup> The kinetic modeling of this system is complex because several reactions occur simultaneously in parallel and consecutive ways (Figure 1). Besides, humins production is complex to track. It is vital to have reliable kinetic and thermodynamic models to draw process flow diagrams for alkyl levulinate production. From the knowledge of these models, it is possible to determine the optimum reaction conditions.

The kinetics of 5-HMF alcoholysis is in central position in the reaction scheme (Figure 1), because it can lead to the production of LA or BL. By considering solely the butanolysis of 5-HMF, one can evaluate the production of humins from 5-HMF at different operating conditions. To the best of our knowledge, such model was not developed for the production of butyl levulinate over heterogeneous catalysts.

This manuscript proposes to study the kinetics of 5-HMF butanolysis over Amberlite IR-120. Indeed, Ramirez et al.,<sup>39</sup> showed the benefit of using cation exchange resin to produce BL from fructose butanolysis. Also, Di Menno Di Bucchianico et al.,<sup>41</sup> showed the benefits of using Amberlite IR-120 and  $\gamma$ -valerolactone (GVL) as a co-solvent for the kinetics of fructose butanolysis. The second stage of this manuscript is the development of kinetic models to explain the reaction mechanism. Special attention was paid to vary widely the 5-HMF loading, catalyst loading and reaction temperature. The knowledge of a kinetic model for concentrated 5-HMF solution is important for the alcoholysis of concentrated sugar solution. Besides,

independent esterification experiments were performed to ease the estimation stage. A cross-validation stage was included to evaluate the developed models.

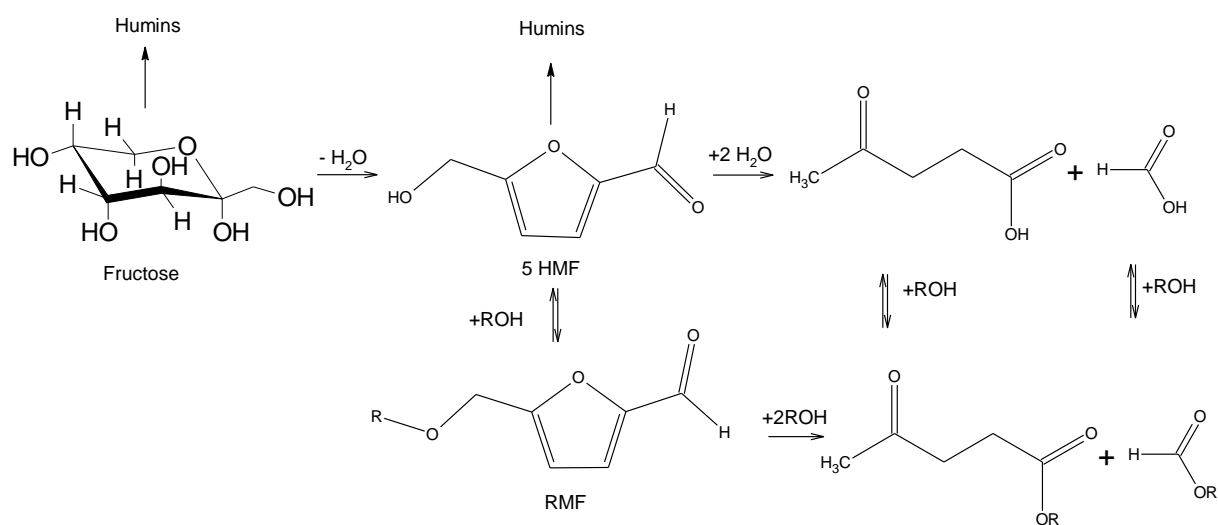


Figure 1. Reaction steps for the alcoholysis of fructose.<sup>53</sup>

## 2. Experimental section

### 2.1 Chemicals

5-(hydroxymethyl)furfural (5-HMF, 99% purity), 5-(ethoxymethyl)furfural (EMF, 97% purity), levulinic acid (LA,  $\geq 97\%$  purity), formic acid (FA,  $\geq 95\%$  purity) and  $\gamma$ -valerolactone ( $\geq 99\%$  purity) were purchased from Sigma-Aldrich. 1-Butanol (BuOH,  $\geq 99.5\%$  purity), butyl levulinate (BL,  $\geq 98\%$  purity), butyl formate (BF,  $\geq 97\%$  purity) and acetone ( $\geq 99.9\%$  purity) from VWR chemicals. Amberlite IR120 H<sup>+</sup> form (ion-exchange resin, native harmonic mean size: 0.620 to 0.830 mm) commercial catalyst was provided by Acros Organics. Nitrogen gas (N<sub>2</sub> purity > 99.999 vol%) came from Linde. All chemicals were employed without further purification.

### 2.2 Analytical methods

Reaction samples were diluted in acetone and analysed by gas chromatograph Bruker Scion 456-GC, equipped with a VF-1701ms Agilent column (60.0 m length x 250  $\mu$ m inner diameter x 0.25  $\mu$ m film thickness) and a flame ionization detector (FID). The injector was set with a temperature of 250 °C, injection volume of 1  $\mu$ L and split ratio of 1:20. Helium (>99.999 vol%) is used as carrier gas at a constant flow rate of 1.0 mL/min to transfer the sample from the injector, through the column and into the FID-detector, whose temperature was set to 250 °C. The oven temperature was programmed from 40 °C to 240 °C with 20 °C/min of ramp rate. Reference samples with standard solutions of pure 5-HMF, LA, EMF, BL and BF were used as standards to prepare daily calibration curves. EMF was used as standard for BMF due to its commercial unavailability. A repetition of three injections for each sample was considered to estimate the uncertainty, measured by the standard deviation, in the analytical method. In this study, the standard deviation for the different concentrations was lower than 0.03 mol/L.

### 2.3 Kinetic experiments

Under isothermal and isobaric conditions, kinetic experiments were carried out in a 300 mL Parr stainless steel batch reactor, equipped with an electric heating system. The presence of a gas entrainment impeller (diameter 2.5 cm) with a hollow shaft provided a uniform mixing of

the reacting mixture. As shown in Table 1, the reactor was loaded with HMF initial mass varying between 1.6 and 7 g, catalyst mass up to 15.3 g and a fixed solvent volume of butanol-GVL with ratio 70:30 wt%.<sup>41</sup> In runs 10-16, levulinic acid and levulinic-formic acid mixture esterification (initial concentration range 0.05 – 0.5 mol/L) were performed in the same solvent system and by using the same catalyst, i.e, Amberlite IR-120. Nitrogen was used to pressurize the system at 20 bars to limit gas-liquid partition of the liquid phase.<sup>41</sup> Rotation speed was set to 800 rpm, since previous studies on fructose butanolysis by using Amberlite IR120 in the same apparatus have demonstrated the negligibility of external and internal mass transfer limitations by using the native catalyst particle size distribution at this rotation speed.<sup>41</sup> Amberlite IR120 was pre-treated as described by Di Menno Di Bucchianico et al.<sup>41</sup> The catalyst was washed with distilled water and, then with pure butanol, before being dried in an oven at 90 °C for 5 hours under atmospheric pressure. For each kinetic experiment (Table 1), we used fresh catalysts. Catalyst reusability was also tested by re-treating the used-catalyst, as described above, before reusing it in a second run. In kinetic runs, temperature was set between 80 and 115 °C, without exceeding 120 °C. Indeed, sulfonic active sites from Amberlite IR-120 can leach for temperature higher than 120°C. During the heating phase, the temperature ramp of the system has been recorded for each experiment. After a first sample collected at ambient temperature to measure the initial concentration of the loaded reagents, intermediate samples were collected to monitor the catalytic reaction, since the catalyst was loaded into the system at the beginning and therefore in contact with the reagents during the heating step. Once the set temperature was reached, a sample was taken and the next ones at 5 min, 30 min, and then every hour for up to 7 h.

Table 1. Experimental matrix

Exp.	Temp. °C	mHMF <sub>0</sub> g	mBuOH <sub>0</sub> g	mGVL <sub>0</sub> g	m <sub>dried</sub> cat. g	mLA <sub>0</sub> g	mFA <sub>0</sub> g	[GVL] <sub>0</sub> mol.L <sup>-1</sup>	[BuOH] <sub>0</sub> mol.L <sup>-1</sup>	[HMF] <sub>0</sub> mol.L <sup>-1</sup>	[LA] <sub>0</sub> mol.L <sup>-1</sup>	[FA] <sub>0</sub> mol.L <sup>-1</sup>
1	110	1.6	85.2	36.5	4.9	0.00	0.0	2.40	7.57	0.08	0.00	0.00
2	100	1.6	85.2	36.5	4.9	0.00	0.0	2.40	7.57	0.08	0.00	0.0
3	90	1.6	85.2	36.5	4.9	0.00	0.0	2.40	7.57	0.08	0.00	0.00
4	110	7.0	85.2	36.5	8.0	0.00	0.0	2.31	7.27	0.31	0.00	0.00
5	100	3.0	85.2	36.5	9.2	0.00	0.0	2.38	7.49	0.16	0.00	0.00
6	100	3.0	85.2	36.5	4.9	0.00	0.0	2.38	7.49	0.15	0.00	0.00
7	80	3.0	85.2	36.5	4.9	0.00	0.0	2.38	7.49	0.15	0.00	0.00
8	85	7.0	85.2	36.5	8.0	0.00	0.0	2.31	7.27	0.32	0.00	0.00
9	105	3.0	85.2	36.5	10.0	0.00	0.0	2.38	7.49	0.14	0.0	0.00
10	80	0.0	80.9	34.7	4.0	8.13	0.0	2.28	7.17	0.00	0.51	0.00
11	95	0.0	80.9	34.7	4.0	8.13	0.0	2.28	7.17	0.00	0.51	0.00
12	110	0.0	80.9	34.7	3.0	8.13	0.0	2.28	7.17	0.00	0.51	0.00
13	80	0.0	84.0	36.0	2.0	1.64	0.63	2.39	7.53	0.00	0.10	0.09
14	110	0.0	84.0	36.0	2.0	1.63	0.64	2.39	7.53	0.00	0.10	0.09
15	95	0.0	84.5	36.3	6.0	1.00	0.40	2.40	7.57	0.00	0.06	0.06
16	100	0.0	84.0	36.0	8.0	1.63	0.64	2.39	7.53	0.00	0.12	0.09
17	100	5.0	85.2	36.5	15.3	0.00	0.0	2.34	7.37	0.28	0.00	0.00
18	115	3.0	85.2	36.5	10.0	0.00	0.0	2.37	7.49	0.17	0.00	0.00
19	100	3.0	85.2	36.5	1.0	0.00	0.0	2.37	7.49	0.17	0.00	0.00
20	100	3.0	85.2	36.5	0.0	0.00	0.0	2.37	7.49	0.17	0.00	0.00

### 3. Results

#### 3.1 Repeatability

Besides analyzing each sample three times, two experiments were repeated: 1 and 6. Figures S1.1 shows the normalized ratio of each species to the initial HMF concentration calculated at initial reaction temperature (ambient temperature) versus time ( $\frac{[HMF]}{[HMF]_0}$ ,  $\frac{[LA]}{[HMF]_0}$ ,  $\frac{[BMF]}{[HMF]_0}$  and  $\frac{[BL]}{[HMF]_0}$ ) for Experiment 1 and 1-repeated. One can notice that kinetic profiles are similar for both experiments. Also, LA concentration is lower than BL or BMF concentrations.

Figures S1.2 display the kinetic profiles for the different species during the alcoholysis of 5-HMF. One can observe that Experiment 6 and 6-repeated are similar from a kinetic standpoint.

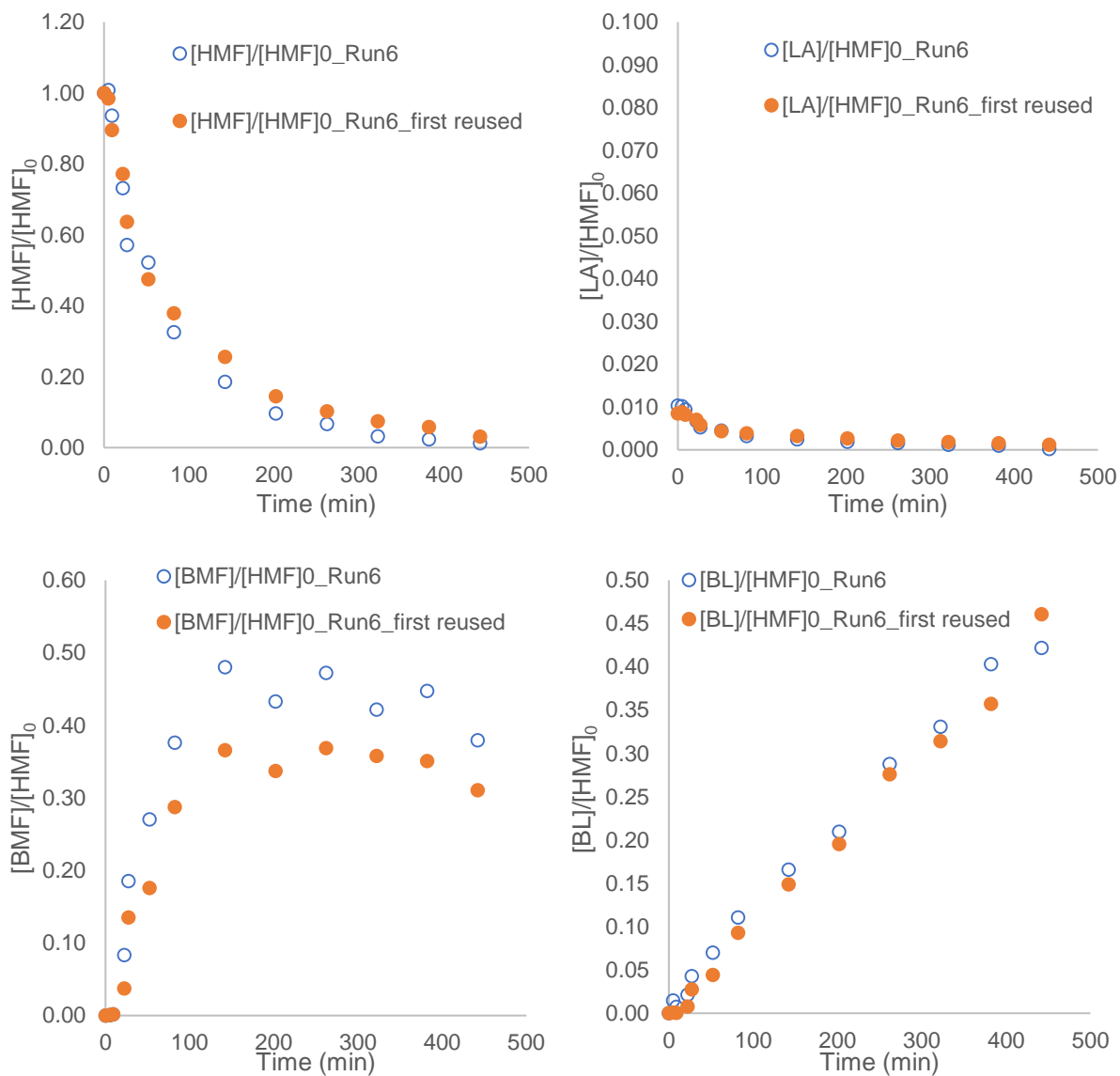
Concentrations displayed in Figures S1.1 and S1.2 confirm that our experimental procedure is repeatable, which is essential to estimate kinetic constants from experimental data.

#### 3.2 Catalyst reused

We reused the catalyst from Run 6, and tested the catalyst reuse in the same operating conditions. Figures 2 show the kinetic profiles for each species. The evolution of the normalized concentrations  $\frac{[HMF]}{[HMF]_0}$  versus time are very similar for Run 6 and Run 6 with the first reused.

For the ratio  $\frac{[BMF]}{[HMF]_0}$ , one can notice that the kinetics of BMF generation is slightly affected.

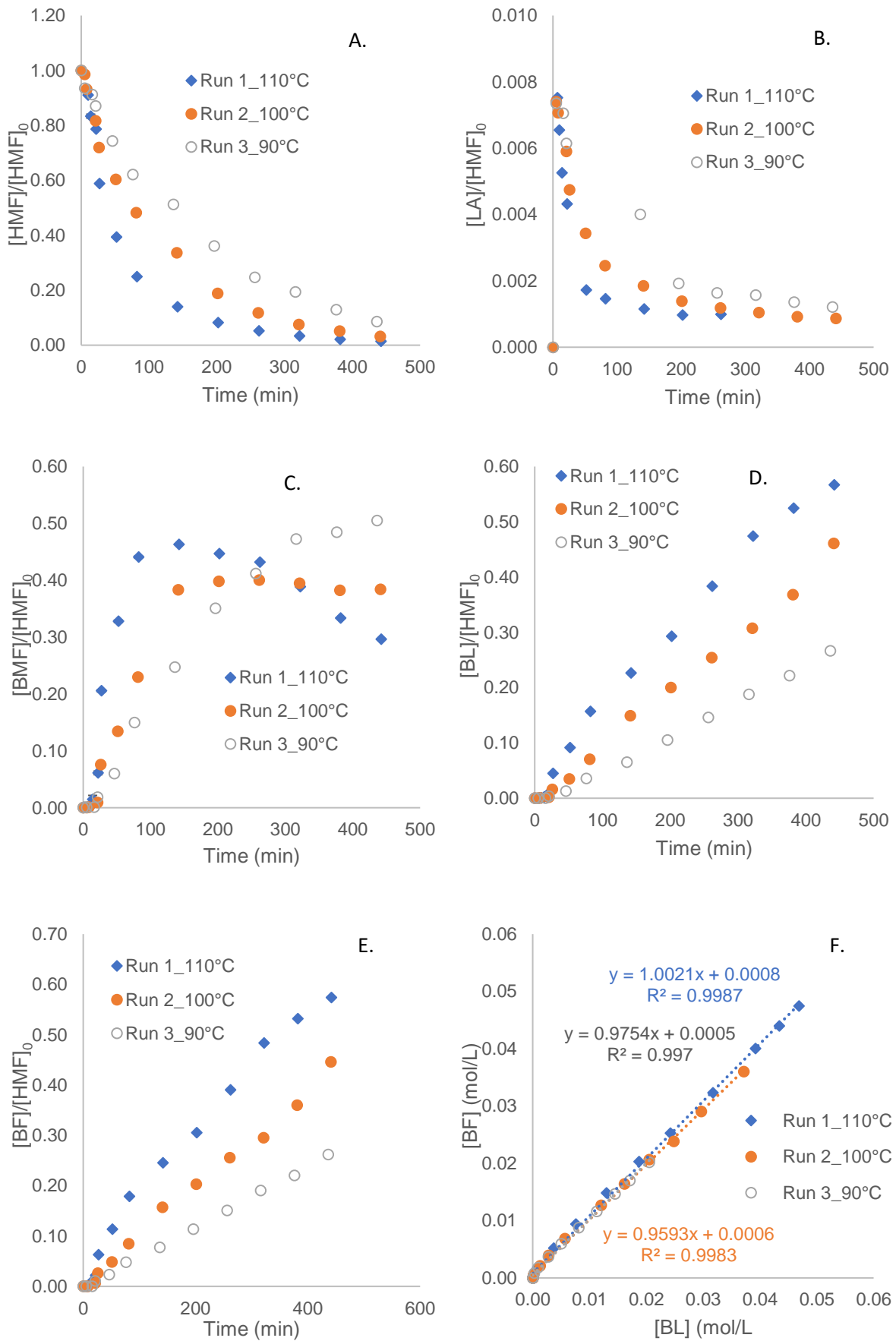
Nevertheless, the ratio  $\frac{[BL]}{[HMF]_0}$  are similar for both experiments, maybe because of the production of BL from LA esterification. Catalyst deactivation can be considered negligible.



Figures 2. Effect of catalyst deactivation on the alcoholysis of HMF-5.

### 3.3 Effect of temperature

The temperature effect on kinetics was studied by comparing Runs 1, 2 and 3. The concentrations versus time were normalized by the initial concentration of 5-HMF. One should keep in mind that it is challenging to compare the first 15 minutes, because during this period, the reaction temperature increases to reach the desired temperature. From Figures 3, it is obvious that the kinetics depend on the reaction temperature. As the temperature increases, the kinetics is faster. The rise from 90 to 110 °C accelerates the kinetics of BMF production and consumption into BL and BF. The production of LA can be considered as low (Figure 3B), and one can notice that the kinetics of BL and BF are similar (Figure 3F). This similarity is higher when the temperature increases, meaning that the production of LA from HMF can be considered negligible. Mass balance on the initial concentration of HMF shows a loss of HMF to humins, which varies from 15 to 20%.

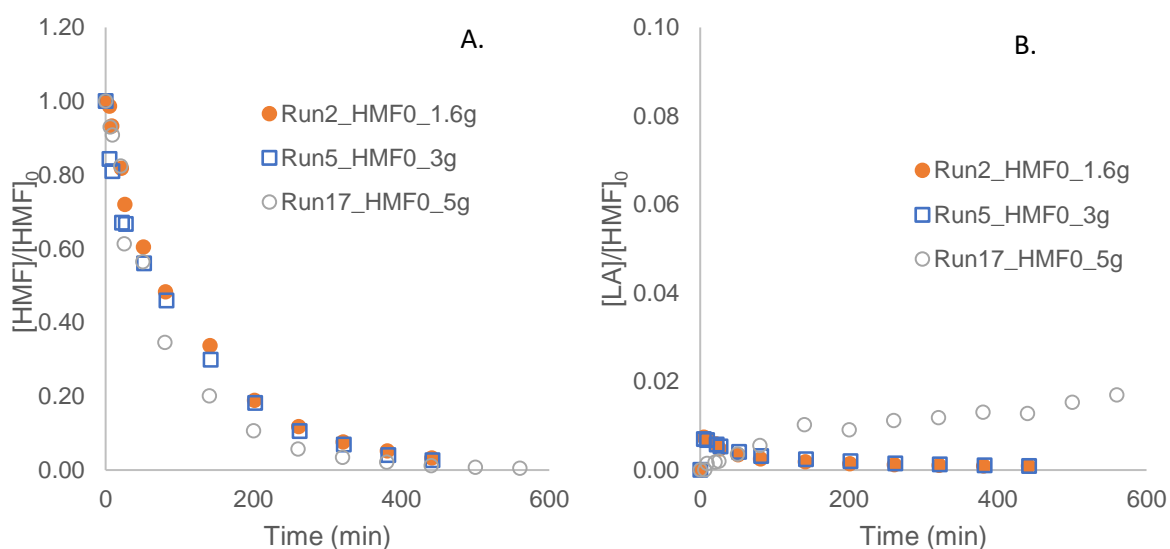


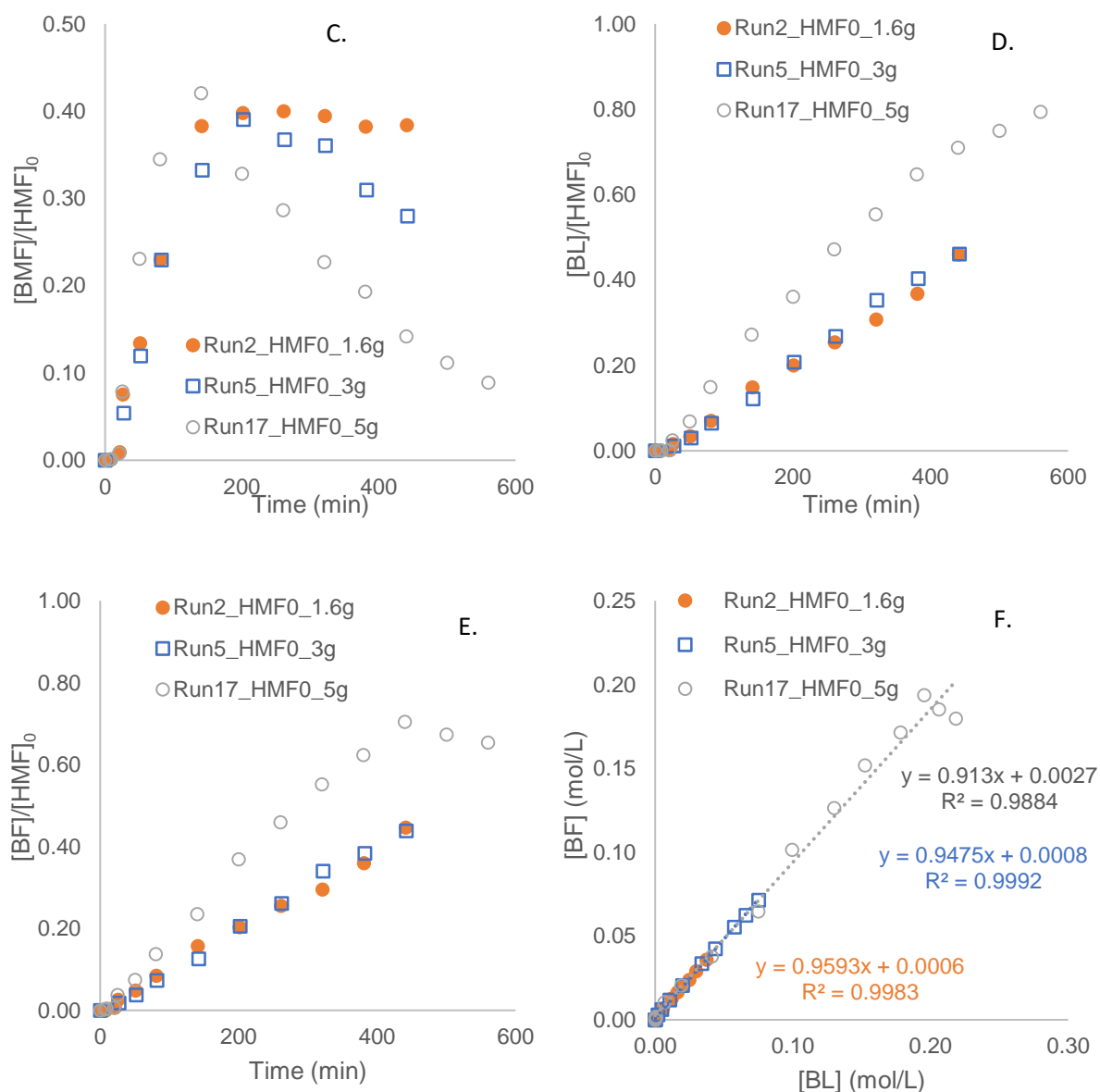
Figures 3. Effect of temperature on the kinetics of HMF-5 alcoholysis.

### 3.4 Effect of 5-HMF loading

To evaluate the effect of HMF loading on the kinetics, Runs 2, 5 and 17 were compared. In these experiments, the molar ratio  $n_{\text{HMF}0}/n_{\text{H}^+, \text{apparent}}$  were kept the same. Figure 4A shows that the kinetics of 5-HMF consumption is slightly faster for high HMF loading, i.e., Run 17. Interestingly, this higher amount of 5-HMF leads to a higher production of LA in Run 17 (Figure 4B), which is usually lower. This significant production of LA decreases the linearity/parity between BL and BF concentrations in Run 17 (Figure 4E). High HMF loading increases the BMF concentration, leading to a higher BL production in Run 17. The linearity decrease between BL and BF in Run 17 is shown in Figures 4D and 4E, where the ratio  $\frac{[\text{BF}]}{[\text{HMF}]_0}$  reached a plateau and not ratio  $\frac{[\text{BL}]}{[\text{HMF}]_0}$ . In Run 17, the fact that the ratio  $\frac{[\text{BF}]}{[\text{HMF}]_0}$  reached a plateau and the increase of the ratio  $\frac{[\text{LA}]}{[\text{HMF}]_0}$  could be linked. If the concentration of LA increases, thus the FA concentration also increases, but the volatility of the latter is higher than LA. Thus, there was less FA than LA in the liquid phase limiting the esterification of FA by butanol to produce BF.

For this series of experiments, the mass balance on the initial concentration of HMF shows a side-reaction of HMF degradation into humins.



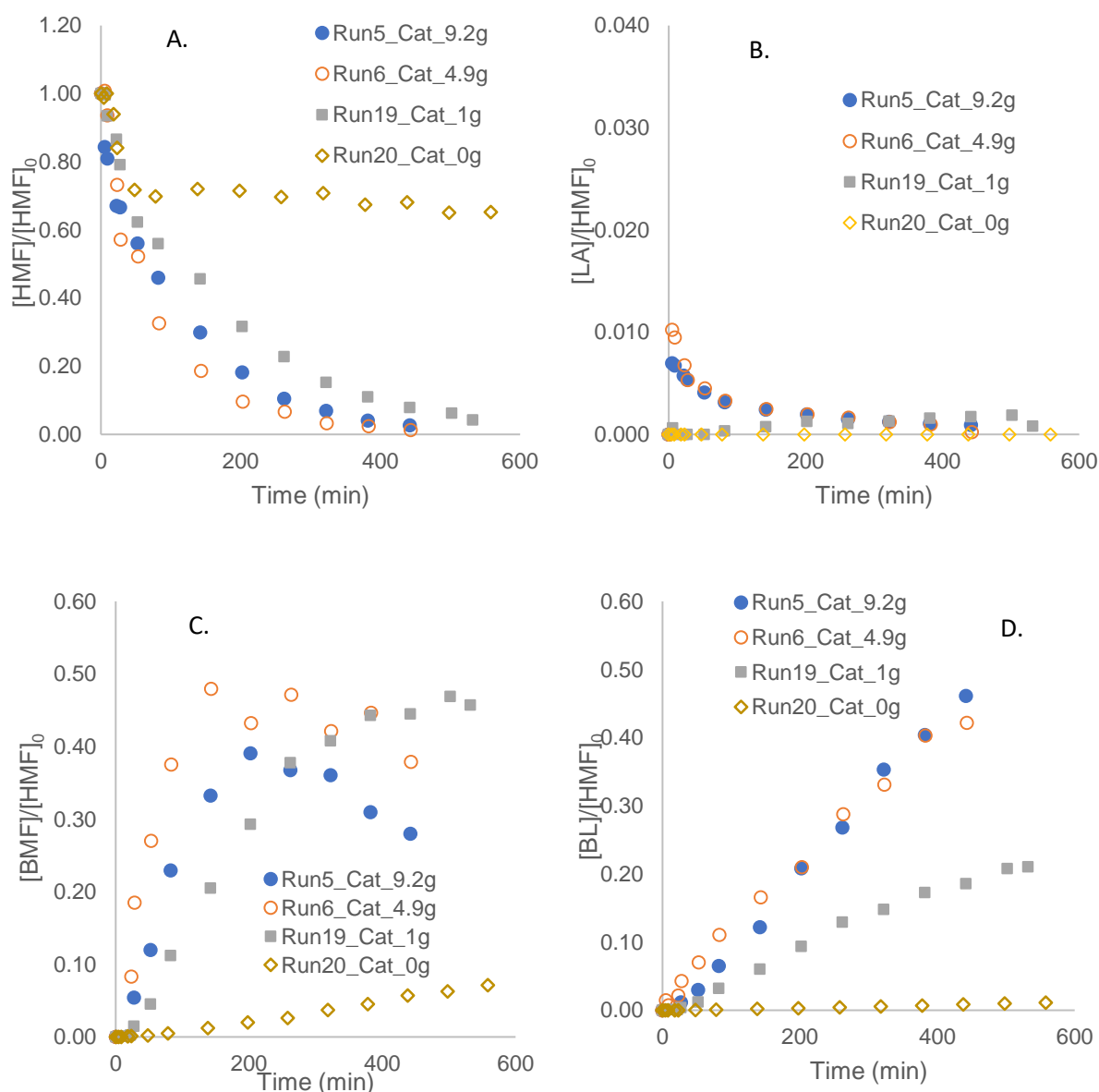


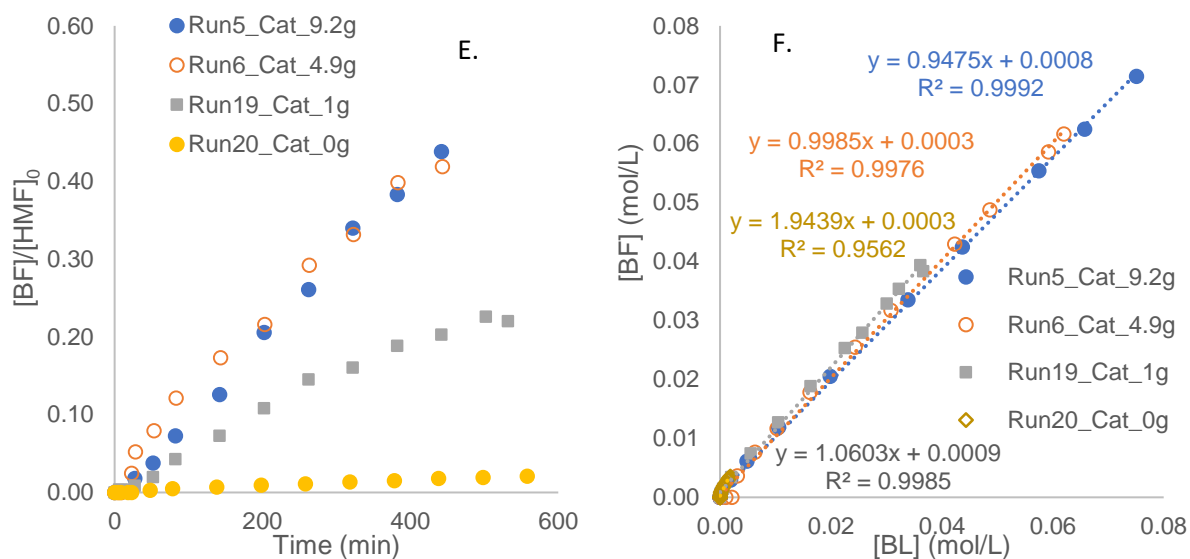
Figures 4. Effect of HMF loading on the kinetics.

### 3.5 Effect of catalyst loading

To evaluate the catalyst loading effect, i.e.,  $\frac{n_{H^+, \text{from Amberlite}}}{V_{\text{Reaction}}}$ , Runs 5, 6, 19 and 20 were compared (Figures 5). From Figures 5, one can observe that the generation kinetics increase from 0 to 4.9 gram of dried catalyst. Then, from 4.9 to 9.2 grams of catalyst, there is no significant effect on the rate of HMF consumption or BL production. For Run 5, the amount of protons is two times higher than the amount of HMF; in other words, more acid sites are available than chemical reactions.

The blank experiment (Run 20) shows that during the first 50 minutes, HMF is consumed, but then the kinetics of decomposition is slower. These two kinetic regimes might be linked to the production of humins and BMF. One cannot say that there are no chemical reactions without acid catalysts. Nevertheless, this production could be initiated by some small amount of proton and then by LA production. Figure 5F shows that in the absence of catalysts, the linearity between BF and BL decreases, which might be due to a longer lifetime of LA and FA. Figures 5 show that protons catalyze each reaction step.

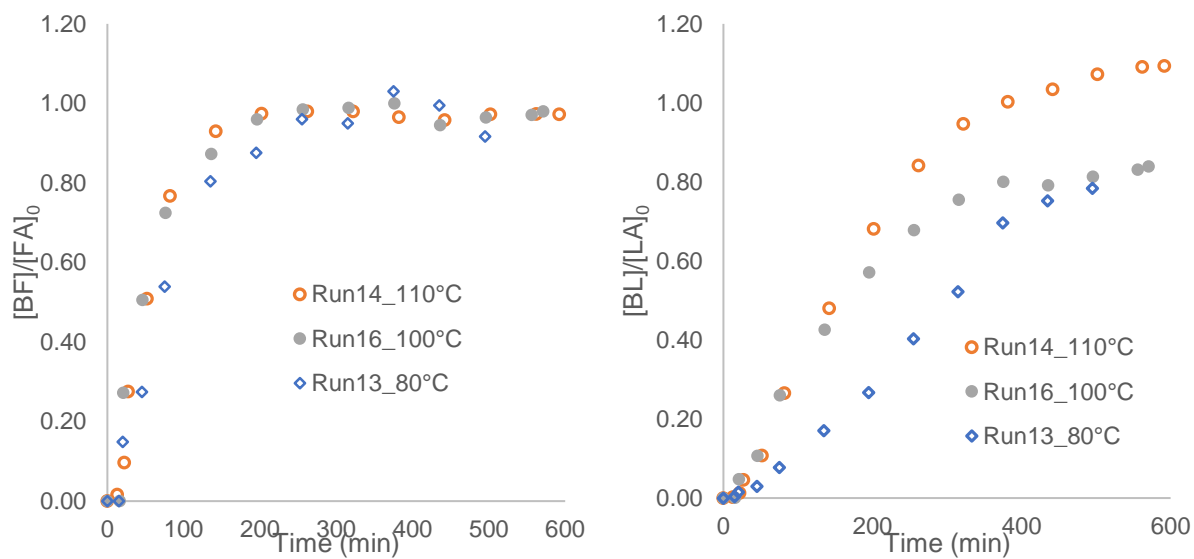




Figures 5. Effect of catalyst loading on the kinetics of HMF butanolysis.

### 3.6 Esterification reactions

The hydrolysis of HMF leads to the production of LA and FA. These species can be esterified into BL and BF. It is very challenging to track the concentrations of LA and FA during the alcoholysis because their concentrations can be low, and FA is volatile. To overcome this issue, we performed independent experiments of esterification using the same solvent environment and LA and FA as starting materials. Figures 6 show the effect of temperature on the kinetics of esterification. One can notice that in these conditions, the esterification reactions can be considered irreversible because no water was added to the reaction mixture. The kinetics of FA esterification is faster than LA esterification. Interestingly, under these operating conditions, the temperature increase does not significantly affect the rate of esterification for FA esterification.



Figures 6. Effect of temperature on esterification kinetics in the same operating conditions as alcoholysis.

#### 4. Discussion on kinetics

The reaction mechanism of 5-HMF hydrolysis is still under debate. This difficulty is increased by the side-reaction of humin production, where the hydroxyl group of 5-HMF plays an important role.<sup>1,52,53</sup> The solvent role also interferes with the kinetics and thermodynamics of this reaction system and its capacity to dissolve 5-HMF or humins.<sup>54</sup> Online analysis to track the different intermediates of this reaction system is cumbersome, so some research groups have used DFT calculation to unravel some elementary steps.<sup>51,55,56</sup>

From the Results section, one can consider that all esterification reactions are irreversible and humins production must be considered in these operating conditions. The fact that esterification are irreversible in this system is due to the very low concentration of water, i.e., no water was added. We assumed that the etherification of HMF to BMF is an irreversible reaction.

Figure 7 shows a simplified reaction scheme for the production of BL from 5-HMF alcoholysis.

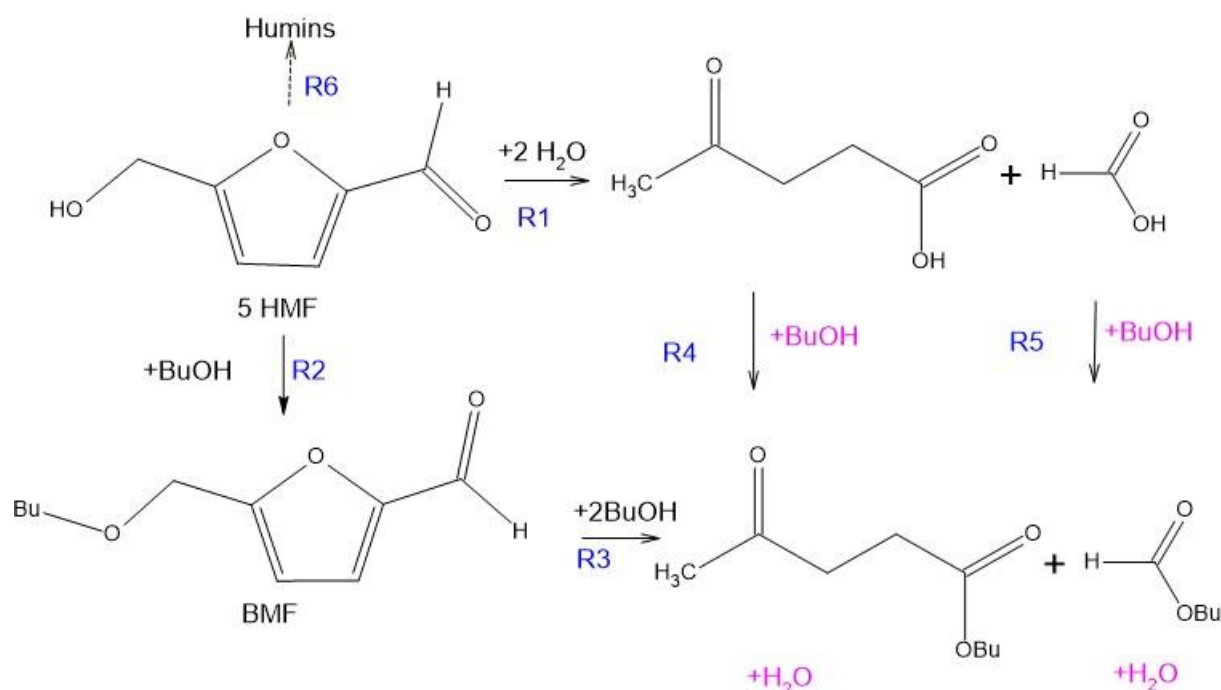


Figure 7. Simplified reaction steps for the butanolysis of 5-HMF.

Based on the work of Wang et al.,<sup>51</sup> we have proposed another reaction scheme illustrated in Figure 8. We assumed that there is another rate-determining step before the production of LA and BL.

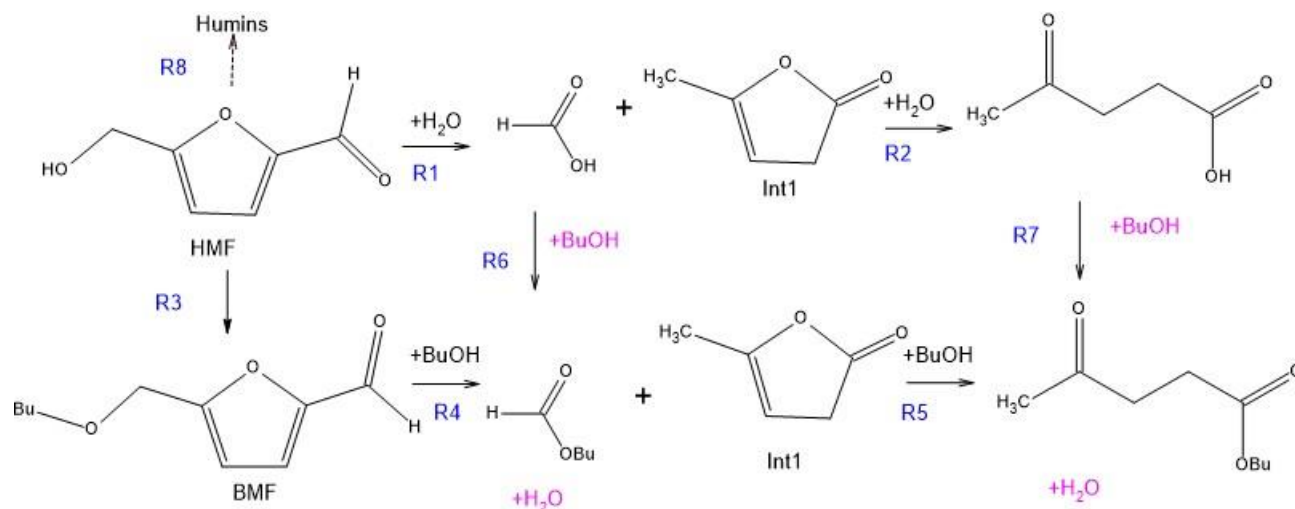


Figure 8. Reaction mechanism considering an intermediate Int1.

Another possible side reaction is the etherification of butanol to dibutyl ether<sup>57</sup>, but such a reaction was not observed in this study. For humins production from 5-HMF, several authors expressed its reaction rate as a first-order according to 5-HMF concentration. If humins production is a polymerization reaction system, this first-order might be wrong. In this manuscript, both orders will be evaluated.

All the reaction steps were considered to be catalyzed by the protons from Amberlite IR-120 (Figures 5). The catalytic effect due to LA was considered to be negligible due to the low concentration of LA. A pseudo-homogeneous approach was used to describe the role of proton from the resins.<sup>58</sup> In other words, protons from the sulfonic groups are considered to have a high degree of freedom. The developed models did not consider the adsorption and desorption steps on sulfonic groups. The proton concentration was calculated based on the acid capacity of Amberlite IR-120.<sup>59–61</sup>

$$[Prot.] = \frac{m_{dried\ catalyst} \cdot Capacity \left( \frac{mol\ of\ Proton}{m_{dried\ catalyst}} \right)}{V_{Reaction}} \quad Eq. (1)$$

The volume of reaction  $V_{\text{Reaction}}$  was calculated based on the total mass ratio to the density of butanol at the corresponding temperature.<sup>44</sup> The effect of sampling was taken into account.

## 4.1 Models

Four models were developed based on Figures 6 and 7, and by testing first and second order for humins production rate.

### A. Model 1

From Figures 6, each step was considered an elementary one; thus, the reaction rates can be expressed as

$$R_1 = k_1 \cdot [HMF] \cdot [Prot.] \quad \text{Eq. (2)}$$

$$R_2 = k_2 \cdot [HMF] \cdot [BuOH] \cdot [Prot.] \quad \text{Eq. (3)}$$

$$R_3 = k_3 \cdot [BMF] \cdot [BuOH] \cdot [Prot.] \quad \text{Eq. (4)}$$

$$R_4 = k_4 \cdot [LA] \cdot [BuOH] \cdot [Prot.] \quad \text{Eq. (5)}$$

$$R_5 = k_5 \cdot [FA] \cdot [BuOH] \cdot [Prot.] \quad \text{Eq.(6)}$$

$$R_6 = k_6 \cdot [HMF] \cdot [Prot.] \quad \text{Eq.(7)}$$

Water was not added to the reaction mixture but was present in the atmosphere at an infinitesimal concentration and produced during the reaction. Thus, the quantification of water in this reaction system is not possible. For that reason, water concentration was merged into the rate constant  $k_1$ . The degradation of HMF into humins was assumed to be of first order.

Ideal flow conditions were assumed for the batch reactor. Thus, material balances can be derived as

$$\frac{d[HMF]}{dt} = -R_1 - R_2 - R_6 \quad \text{Eq.(8)}$$

$$\frac{d[BMF]}{dt} = R_2 - R_3 \quad \text{Eq.(9)}$$

$$\frac{d[LA]}{dt} = R_1 - R_4 \quad \text{Eq.(10)}$$

$$\frac{d[BL]}{dt} = R_3 + R_4 \quad \text{Eq.(11)}$$

$$\frac{d[BuOH]}{dt} = -R_2 - 2 \cdot R_3 - R_4 - R_5 \quad \text{Eq.(12)}$$

$$\frac{d[FA]}{dt} = R_1 - R_5 \quad \text{Eq.(13)}$$

$$\frac{d[BF]}{dt} = R_3 + R_5 \quad \text{Eq.(14)}$$

$$\frac{d[Humins]}{dt} = R_6 \quad \text{Eq.(15)}$$

## B. Model 2

The difference with Model 1 is that reaction R6 was considered to be of second-order with respect to HMF concentration.

$$R_6 = k_6 \cdot [HMF]^2 \cdot [Prot.] \quad \text{Eq.(16)}$$

Material balance is different for HMF and is expressed as

$$\frac{d[HMF]}{dt} = -R_1 - R_2 - 2 \cdot R_6 \quad \text{Eq.(17)}$$

## C. Model3

From Figure 7, each step was considered an elementary one. Thus, the reaction rates can be expressed as

$$R_1 = k_1 \cdot [HMF] \cdot [Prot.] \quad \text{Eq. (18)}$$

$$R_2 = k_2 \cdot [INT1] \cdot [Prot.] \quad \text{Eq. (19)}$$

$$R_3 = k_3 \cdot [HMF] \cdot [BuOH] \cdot [Prot.] \quad \text{Eq. (20)}$$

$$R_4 = k_4 \cdot [BMF] \cdot [BuOH] \cdot [Prot.] \quad \text{Eq. (21)}$$

$$R_5 = k_5 \cdot [INT1] \cdot [BuOH] \cdot [Prot.] \quad \text{Eq.(22)}$$

$$R_6 = k_6 \cdot [FA] \cdot [BuOH] \cdot [Prot.] \quad \text{Eq.(23)}$$

$$R_7 = k_7 \cdot [LA] \cdot [BuOH] \cdot [Prot.] \quad \text{Eq.(24)}$$

$$R_8 = k_8 \cdot [HMF] \cdot [Prot.] \quad \text{Eq.(25)}$$

The degradation of HMF into humins was assumed to be of first-order.

Material balances can be derived as

$$\frac{d[HMF]}{dt} = -R_1 - R_3 - R_8 \quad \text{Eq.(26)}$$

$$\frac{d[BMF]}{dt} = R_3 - R_4 \quad \text{Eq.(27)}$$

$$\frac{d[INT1]}{dt} = R_1 - R_2 + R_4 - R_5 \quad \text{Eq.(28)}$$

$$\frac{d[LA]}{dt} = R_2 - R_7 \quad \text{Eq.(29)}$$

$$\frac{d[BL]}{dt} = R_5 + R_7 \quad \text{Eq.(30)}$$

$$\frac{d[BuOH]}{dt} = -R_3 - R_4 - R_5 - R_6 - R_7 \quad \text{Eq.(31)}$$

$$\frac{d[FA]}{dt} = R_1 - R_6 \quad \text{Eq.(32)}$$

$$\frac{d[BF]}{dt} = R_4 + R_6 \quad \text{Eq.(33)}$$

$$\frac{d[Humins]}{dt} = R_8 \quad \text{Eq.(34)}$$

#### D. Model4

The difference with Model 3 is that reaction R8 was considered to be of second order with respect to 5-HMF concentration.

$$R_8 = k_8 \cdot [HMF]^2 \cdot [Prot.] \quad \text{Eq.(35)}$$

Material balance is different for HMF and can be expressed as

$$\frac{d[HMF]}{dt} = -R_1 - R_3 - 2 \cdot R_8 \quad \text{Eq.(36)}$$

#### 4.2 Modeling

Simulation and parameter estimation stages were carried out by commercial software Athena Visual Studio.<sup>62,63</sup>

The experimental concentrations of HMF, LA, BMF, BF and BL were used as observables. For such multi-response parameter estimation case, the Bayesian framework is more suitable than the non-linear least squares approach.<sup>64,65</sup> Indeed, the minimization of the objective function requires the determination of the determinant criterion.<sup>66</sup>

The Ordinary Differential Equations (ODEs) issued from material balances were integrated by the DDAPLUS solver, included in Athena Visual Studio software. This solver is developed based on a modified Newton algorithm.<sup>67</sup>

The minimization of the objective function (OF), the determination of the credible intervals for each estimated parameter and the calculation of the normalized parameter covariance were done by the subroutine GREGPLUS.

GREGPLUS uses successive quadratic programming to minimize OF.<sup>63,65</sup>

$$OF = (a + b + 1) \cdot \ln|v| \quad \text{Eq.(37)}$$

where,  $b$  is the number of responses,  $a$  is the number of events in response, and  $|v|$  is the determinant of the covariance matrix of the responses. Each element of this matrix is

$$v_{ij} = \sum_{u=1}^n [C_{iu} - \hat{C}_{iu}] \cdot [C_{ju} - \hat{C}_{ju}] \quad \text{Eq.(38)}$$

with  $C_{iu}$  the experimental concentration and  $\hat{C}_{iu}$  the estimated value for response  $i$  and event  $u$ ;  $C_{ju}$  the experimental concentration and  $\hat{C}_{ju}$  the estimated value for response  $j$  and event  $u$ .

The interval estimates for each estimated parameter are calculated from the final quadratic expansion of the OF. The uncertainty of the estimated parameters was evaluated by the marginal highest posterior density (HPD), which was calculated by GREGPLUS package.

The temperature dependence of rate constants was expressed by a modified Arrhenius equation. Indeed, there is a strong correlation between the pre-exponential factor and activation energy. This strong correlation can increase the confidence intervals, and thus the uncertainty. To avoid such effect, Buzzi-Ferraris recommended to linearize the Arrhenius equation,<sup>68</sup> hence the following expression was used to express rate constants,

$$k(T) = \exp \left[ \ln \left( k(T_{ref}) \right) + \frac{E_a}{R \cdot T_{ref}} \cdot \left( 1 - \frac{T_{ref}}{T} \right) \right] \quad \text{Eq.(39)}$$

where  $T_{ref}$  is the reference temperature, which was the median of the different reaction temperatures.

Preliminary modeling shows that Runs 19 and 20 could not be modeled correctly. Run 20 was performed without catalyst, and 19 was performed with low catalyst loading. The reaction mechanism in the presence of a low amount of Brønsted acid sites is different (Figures 5), thus they were discarded in the modeling stage.

Our modeling strategy included some kinetic experiments with only esterification reactions (Table 1) in the same operating conditions as the butanolysis ones. This inclusion was due to the fact that LA and FA concentrations were low, and thus the estimation of their rates constants just from BL and BF could lead to some estimation bias.

Table 2 summarizes the sum of squared residuals (SSR) for each compound and model, the number of estimated parameters for each model, the Akaike Information Criterion for each model,<sup>20,69</sup> and coefficients of determination for each compound.

It is complicated to find the best model based on SSR or R<sup>2</sup> values (Table 2). Therefore, the criterion AIC was also used.

$$AIC = \text{Number of independent events} \cdot \ln \left( \frac{SSR}{\text{Number of independent events}} \right) + 2 \cdot \text{Number of estimated parameters} \quad \text{Eq.(40)}$$

This criterion takes into account the number of estimated parameters. Lower is the AIC value, and higher is the model quality. Table 2, one can notice that Model 3 is more reliable than the others.

The values of the estimated constants as well as the credible intervals are given in Table S2.1 and Table S2.2 (Supporting information S2). In Table S2.3, the estimated activation energies obtained from this work and found in literature<sup>45-50</sup> are displayed. It is not possible to compare the activation energies, because solvent/reactant and proposed models by other authors (reaction rate expression) were not the same.

For Models 1 and 2, one can consider that the credible intervals are low, meaning that the values were well identified. The credible intervals for the estimated kinetic constants for the hydrolysis of 5-HMF (Step 1) and esterification of FA was slightly wider, which is due to the low concentration of LA and FA. For Models 3 and 4, the credible intervals are wider for the transformation of Int1 to LA and FA and to BL and BF. These wider credible intervals are linked to the fact that the concentration of Int1 was not tracked.

Parity plots for each observable and each model are displayed in Supporting information (S3). One can notice that parity is good for HMF, LA, BF and BL concentrations because the coefficient of determination is higher than 0.95. The parity between experimental and estimated BMF concentrations is slightly lower, i.e., R<sup>2</sup> is ca. 0.9. The mechanism could explain this lower value from HMF to BMF is more complex.

Residual plots for each compound and model are displayed in Supporting information (S4). One can notice that residual values versus experimental and estimated concentrations are randomly distributed, meaning that the defined rate equations were well identified.

Correlation matrix for the estimated parameters were included in Supporting information (S5). The estimated parameters were not correlated to each other because all binary correlation coefficients are lower than 0.95.<sup>70</sup>

Table 2. Summary of modeling results.

	Model 1	Model 2	Model 3	Model 4
Number of Parameters	12	12	16	16
SSR_HMF	0.11	0.12	0.11	0.12
SSR_BMF	0.08	0.09	0.08	0.09
SSR_LA	0.09	0.10	0.08	0.08
SSR_BL	0.21	0.20	0.21	0.20
SSR_BF	0.03	0.03	0.03	0.03
SSR_all	0.52	0.54	0.51	0.53
AIC	-23435	-23312	-23495	-23378
R <sup>2</sup> _HMF	0.97	0.96	0.97	0.96
R <sup>2</sup> _BMF	0.89	0.89	0.90	0.89
R <sup>2</sup> _LA	0.99	0.99	0.99	0.99
R <sup>2</sup> _BL	0.97	0.97	0.97	0.97
R <sup>2</sup> _BF	0.98	0.98	0.98	0.98

The fit of Model 3 to some experimental data are shown in Figures 9-15. A general overview shows that Model 3 can fit the experimental concentrations in different operating conditions such as low 5-HMF loading (Experiment 3, Figures 14), high 5-HMF loading (Experiments 8 and 17; Figures 9 and 12), low reaction temperature (Experiment 3; Figure 14), high reaction temperature (Experiment 18; Figures 13) and high catalyst loading (Experiment 17; Figures 12).

In the case of 5-HMF-free experiments (Experiments 14 and 16; Figures 11 and 15), Model 3 slightly underestimates experimental concentrations of BL and BF for Experiment 14, but overestimates the BL experimental concentrations for Experiment 16.

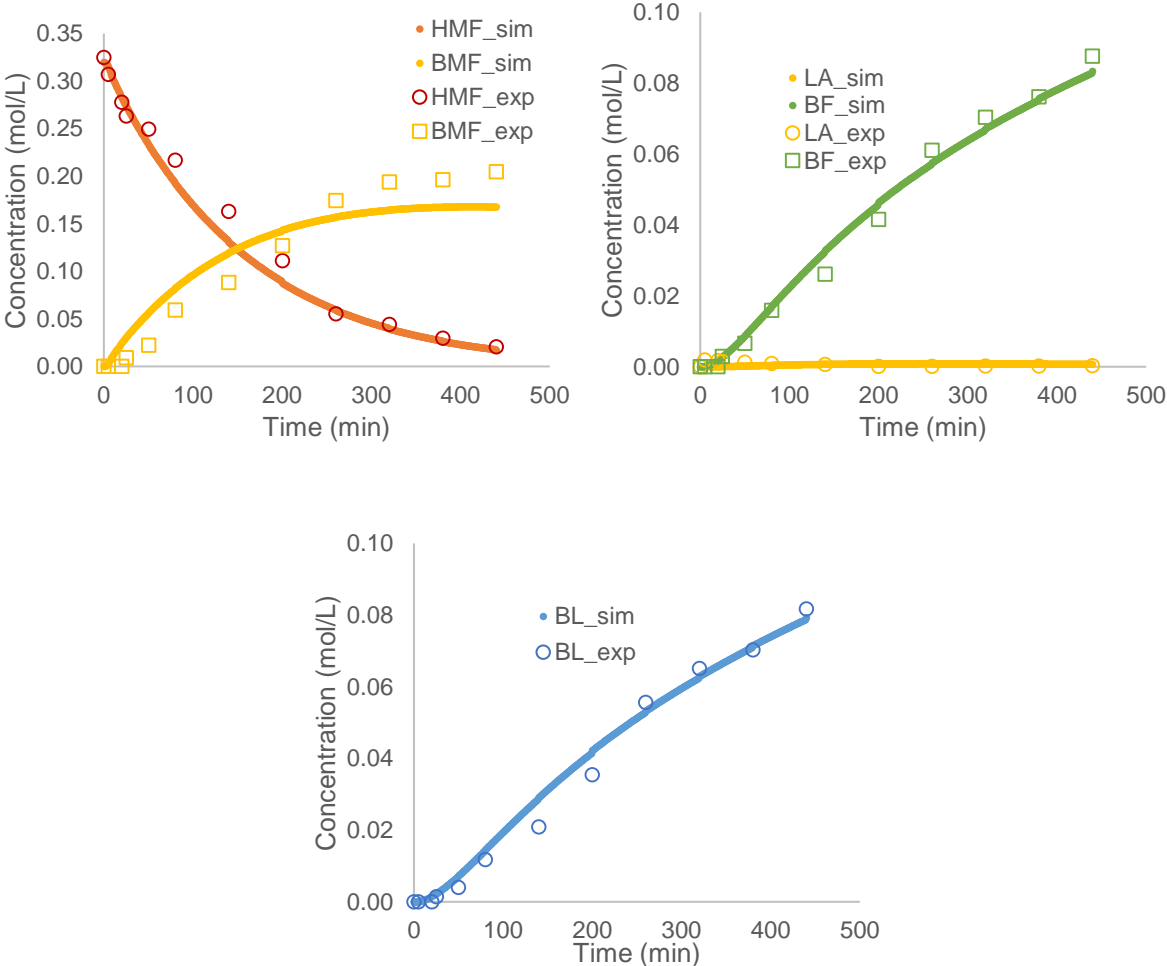


Figure 9. Fit of Model 3 to experimental concentrations (Experiment 8).

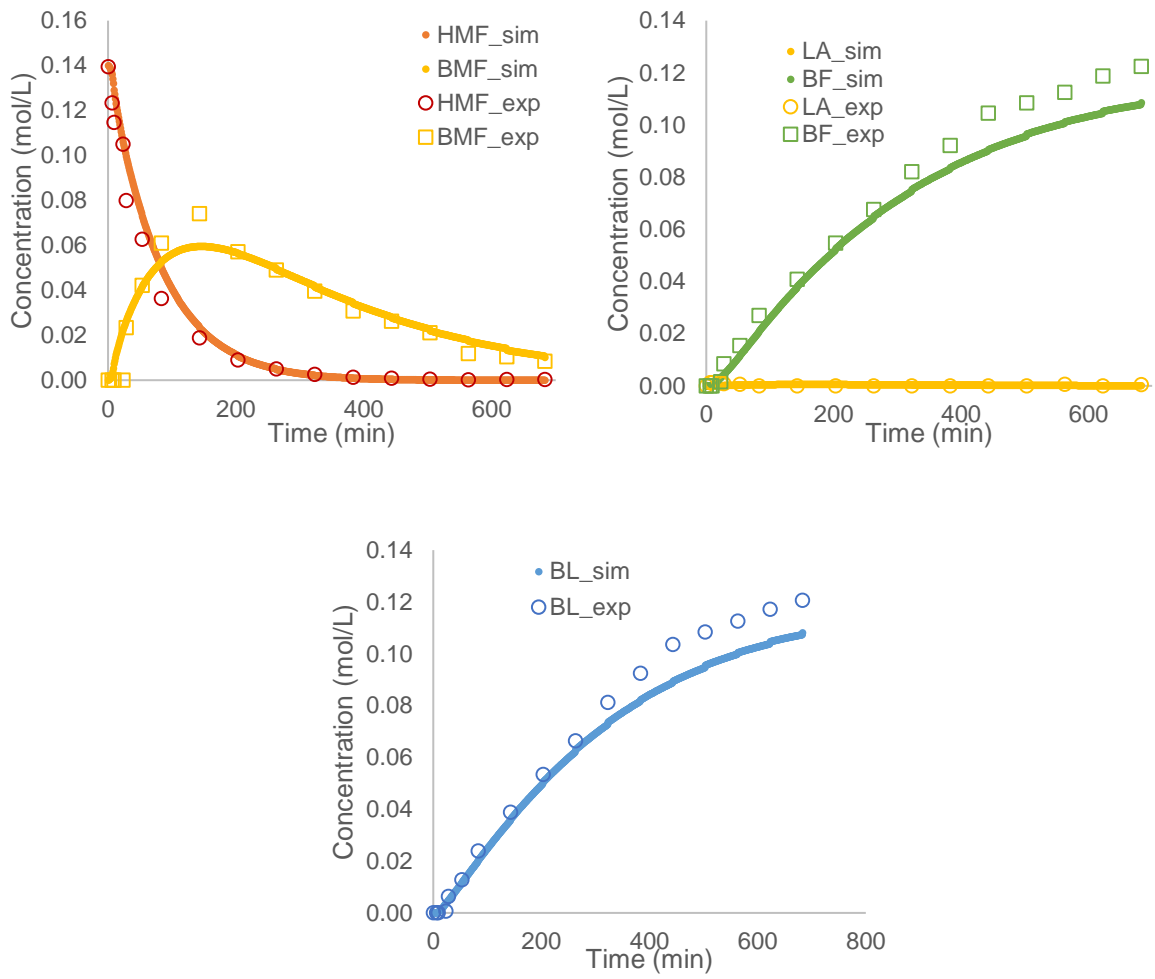


Figure 10. Fit of Model 3 to experimental concentrations (Experiment 9).

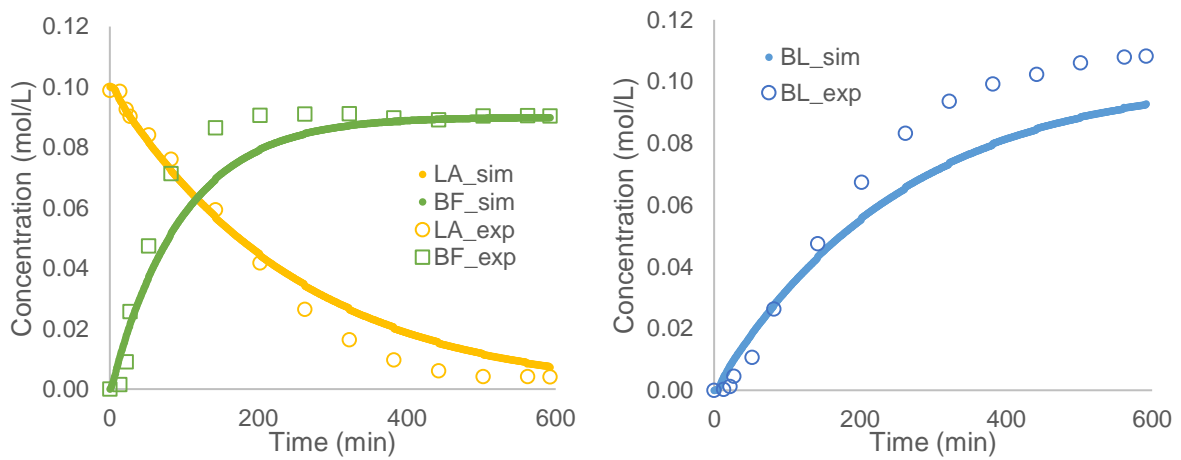


Figure 11. Fit of Model 3 to experimental concentrations (Experiment 14)

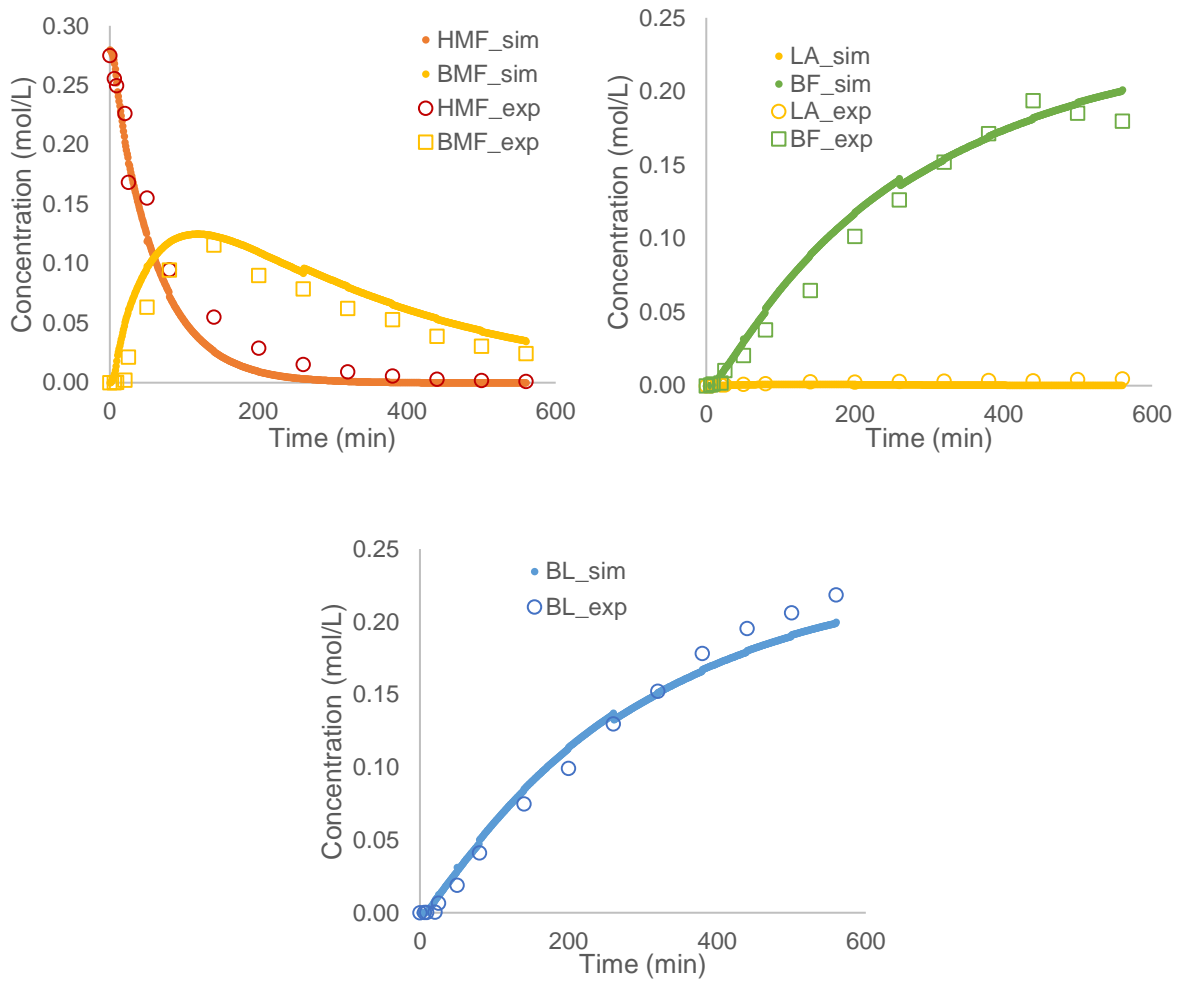
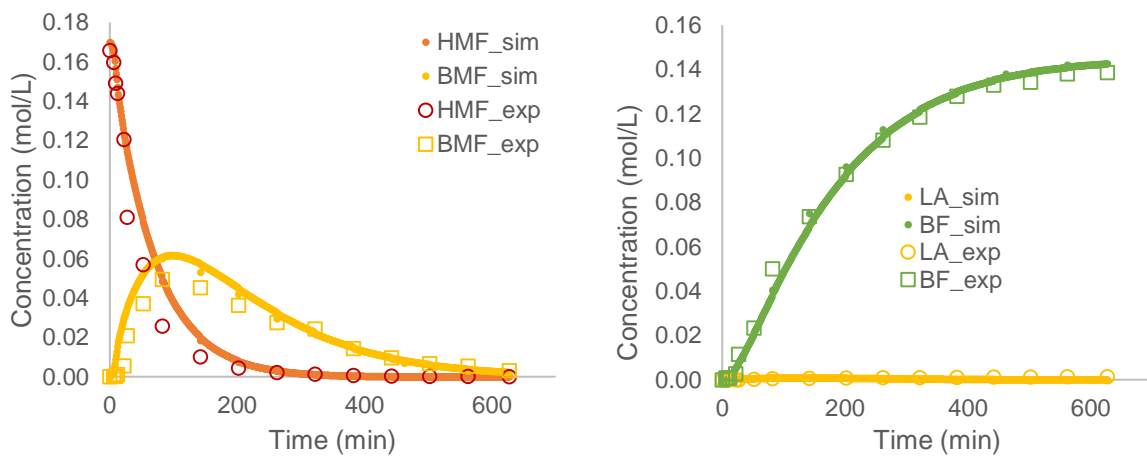


Figure 12. Fit of Model 3 to experimental concentrations (Experiment 17)



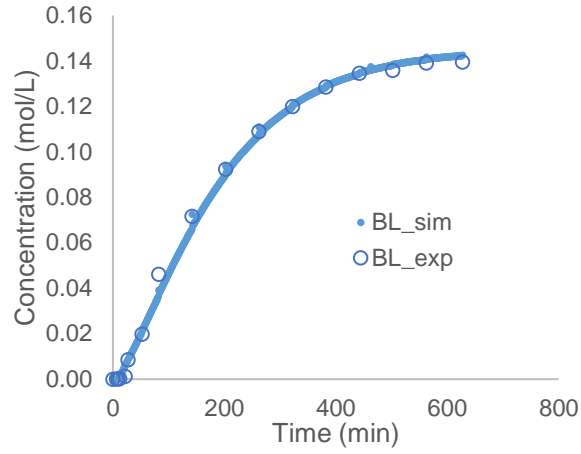
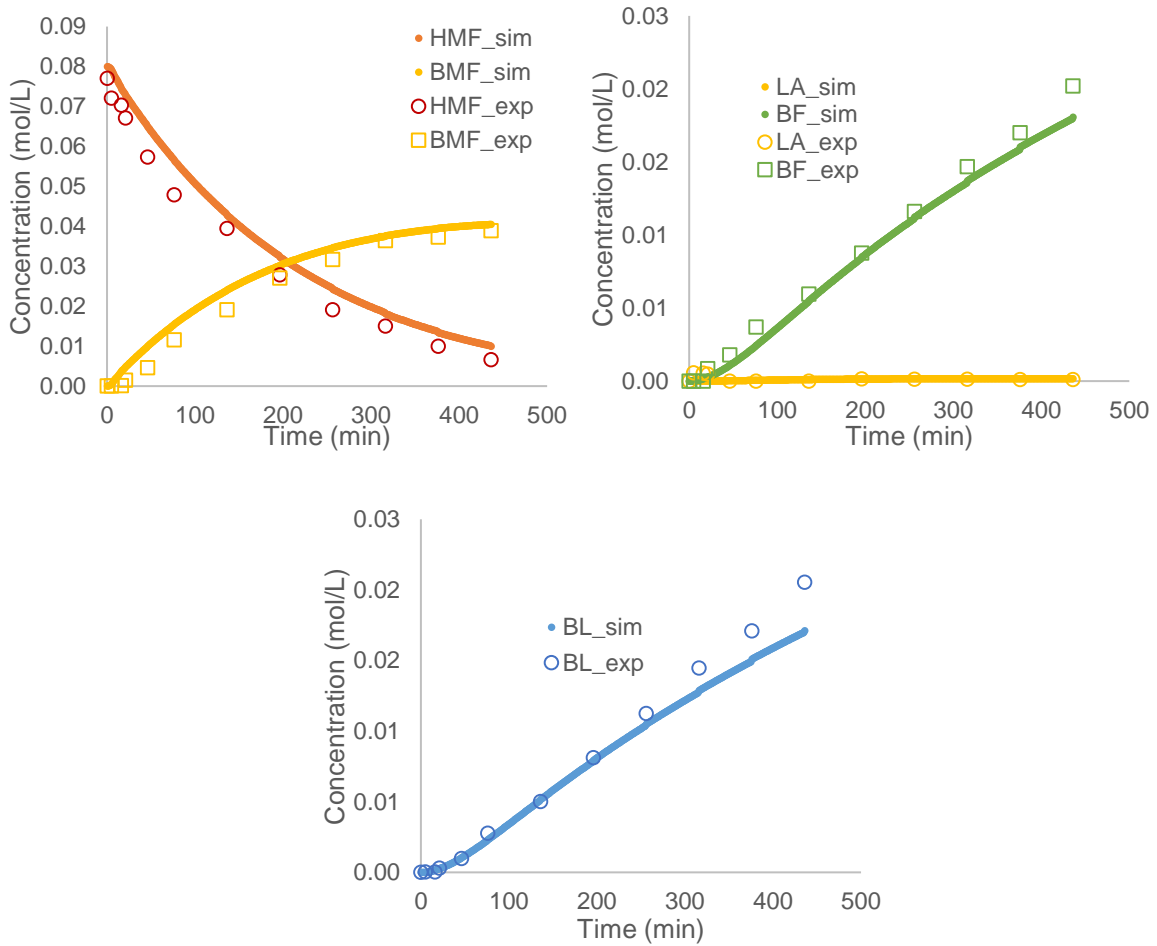


Figure 13. Fit of Model 3 to experimental concentrations (Experiment 18).



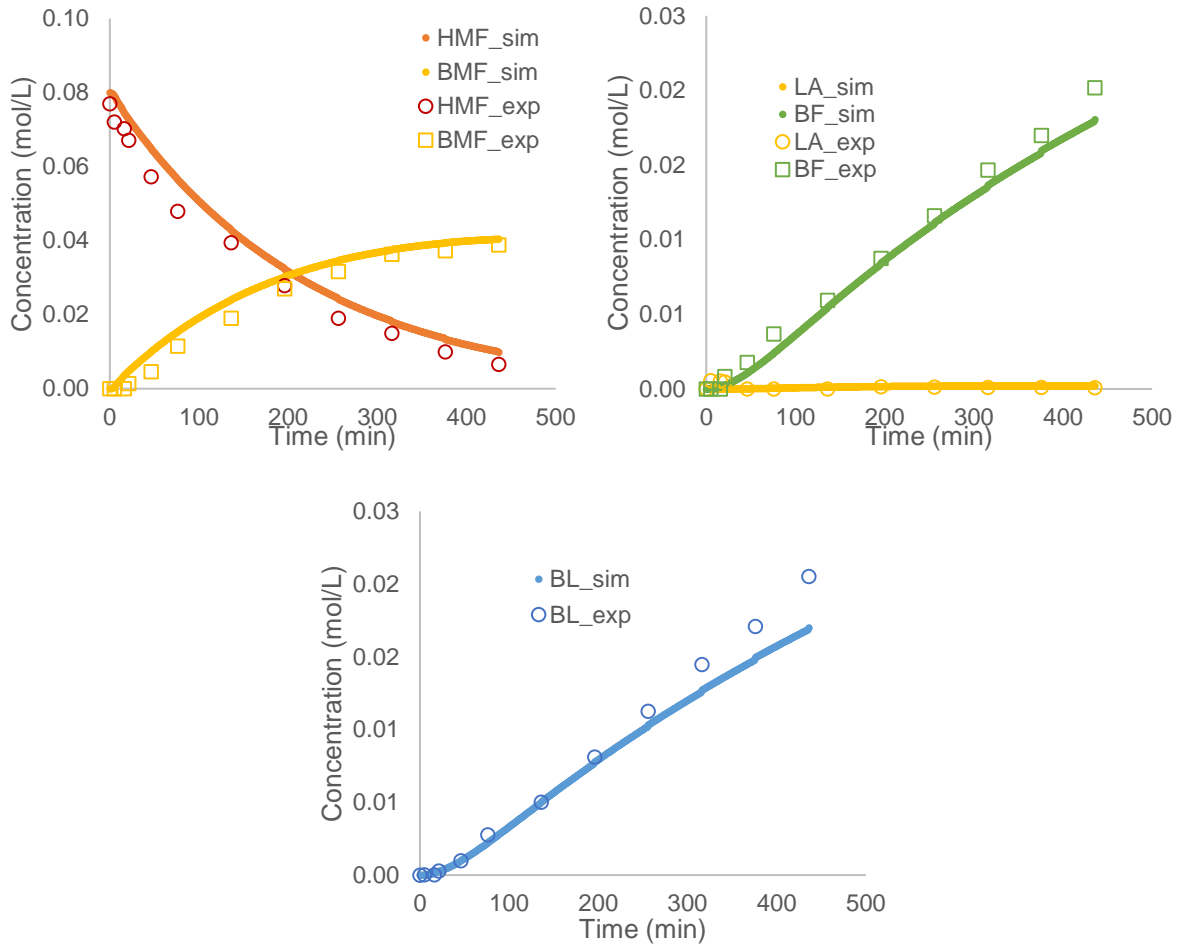


Figure 14. Fit of Model 3 to experimental concentrations (Experiment 3).

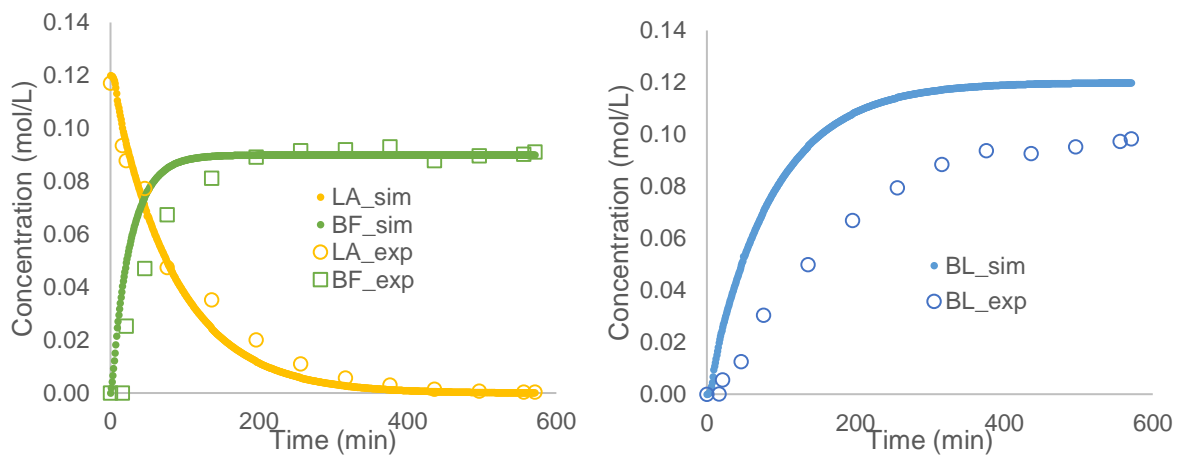


Figure 15. Fit of Model 3 to experimental concentrations (Experiment 16).

### 4.3 Cross-validation

The validation stage is important to finalize the assessment of the different models. A cross-validation approach was used, and more specifically the K-fold method.<sup>71</sup> The 18 experiments were randomly divided into 6 folds (Table 3) by paying attention that each fold contains at least one esterification experiments but not 3. The training (a.k.a regression) were made on 5 folds and testing (a.k.a validation) on the remaining fold as shown by Table 4.

Table 3. Distribution of the 18 experiments in the 6 folds.

Fold	Experiment
Fold 1	12
	11
	5
Fold 2	6
	3
	10
Fold 3	7
	14
	8
Fold 4	16
	4
	17
Fold 5	1
	9
	13
Fold 6	18
	15
	2

Table 4. Different sets for training and testing.

Set	Train	Test
Set 1	Folds 1-2-3-4-5	Fold 6
Set 2	Folds 6-1-2-3-4	Fold 5
Set 3	Folds 5-6-1-2-3	Fold 4
Set 4	Folds 4-5-6-1-2	Fold 3
Set 5	Folds 3-4-5-6-1	Fold 2
Set 6	Folds 2-3-4-5-6	Fold 1

The kinetic constants  $\ln(k(T_{ref}))$  and  $\frac{E_a}{R \cdot T_{ref}}$  for each reaction are estimated from each training stage, and these estimated constants are used for the testing stage. The prediction capacity of a model is evaluated by the  $CV_{(K)}$  number.

$$CV_{(K)} = \frac{1}{7} \cdot \sum_{K=1}^7 (Y_{i,experimental} - Y_{i,simulated})_K^2 \quad \text{Eq. (41)}$$

As the  $CV_{(K)}$  value is low, then the model is predictable. Table 5 shows that  $CV_{(K)}$  numbers are lower for Models 1 and 3.

Table 5.  $CV_{(K)}$  and standard deviation for each model

	<b>Model 1</b>	<b>Model 2</b>	<b>Model 3</b>	<b>Model 4</b>
$CV_{(K)}$	0.130	0.144	0.126	0.248

## 5. Conclusions

The butyl levulinate (BL) production from butanolysis of 5-HMF, without the addition of water, over Amberlite IR-120 was investigated in batch conditions and 20 bars of nitrogen. Butanolysis of 5-HMF is the central reaction system for the production of BL from glucose or fructose butanolysis. GVL was used as a co-solvent. It was found that experiments were repeatable and that catalyst did not undergo any significant deactivation. The analytical investigation showed that 5-(butoxymethyl)furfural (BMF), levulinic acid (LA), butyl formate (BF) and butyl levulinate can be tracked during an experiment. We have also noticed a side-reaction of humins production from mass balance analysis. Preliminary observations showed that the increase of reaction temperature and catalyst loading increase the kinetics of all reaction steps. From our data, esterification reactions were found to be irreversible. The Etherification reaction was assumed to be irreversible.

The second part of this manuscript was to develop and assess different kinetic models to explain the kinetics of this system. The assessment was done via the determination of AIC criteria for each model, and by the use of cross-validation. To ease the parameter estimation stage, independent LA and FA esterification experiments were performed. Operating conditions such as temperature, catalyst and 5-HMF loading were widely varied to develop reliable kinetic model. Basically, two types of models were tested: one with 5 reaction steps and the other one with 8 reaction steps. We have also found that the production of humins was first-order. Based on the evaluation of the statistical output, AIC criterion and the cross-validation stage, it was found that Model 3, i.e., with 8 reaction steps and with a first-order reaction for humins production was the most probable model. Model 3 can simulate the alcoholysis of 5-HMF for experiments with a 5-HMF loadings from 9.7 to 43.7 g/L, a dried Amberlite IR-120 loading from 29.1 to 93.8 g/L and a reaction temperature from 80 to 115°C.

To improve the kinetic model of this reaction system, more investigations are needed to understand the mechanism of humins production and determine which intermediates are formed for the production of levulinates. Using quantum mechanics and advanced analytical techniques could unravel the reaction mechanism for this system and establish accurate material balances.

## Supporting information

This information is available free of charge via the Internet at <http://pubs.acs.org/>.

Repeatability (S1); parameters estimated and from the literature (S2); parity plots (S3); residuals (S4); and correlation matrices (S5).

## Acknowledgments

This investigation was carried out in the framework of the ARBRE project. ARBRE is cofounded by European Union through the European Regional Development Fund (ERDF) and by Normandy Region, via the support of “pôle CTM (Continuum Terre-Mer) and EP2M (Énergies, Propulsion, Matière, Matériaux) de Normandie université”. The Daniele Di Menno Di Bucchianico's doctoral thesis is done in the framework of “ARBRE RIN 100%” funded by Region Normandie, and this thesis is a part of the research activities of “pôle CTM (Continuum Terre-Mer) de Normandie Université”. For the analytical part, this work has been partially supported by University of Rouen Normandy, INSA Rouen Normandy, the Centre National de la Recherche Scientifique (CNRS), European Regional Development Fund (ERDF) N° HN0001343, Labex SynOrg (ANR-11-LABX-0029), Carnot Institute I2C, the graduate school for reasearch XL-Chem (ANR-18-EURE-0020 XL CHEM) and by Region Normandie. GC was financed by FEDER RIN Green Chem 2019NU01FOBC08 Number: 17P04374.

## Notation

$\hat{C}_{iu}$	estimate concentration of specie $i$
$C_{iu}$	experimental concentration of specie $i$
$E_{ai}$	activation energy of reaction $i$ [J/mol]
$k_i$	rate constant of reaction $i$
$n_{H^+}$	number of proton moles
[Prot]	proton concentration [mol/L]
$R_i$	reaction rate $i$ [mol/L/min]
$R$	gas constant [J/K/mol]
$R^2$	coefficient of determination
$T$	temperature [K]
$V_{\text{Reaction}}$	volume of reaction liquid
$ v $	determinant of the covariance matrix of responses

## Abbreviations

AIC	Akaike information criterion
Amb	Amberlite IR-120
BF	Butyl formiate
BL	Butyl levulinate
BMF	5-(butoxymethyl)furfural
BuOH	Butanol
Cat.	Catalyst (Amberlite IR-120)
EMF	5-(ethoxymethyl)furfural
FA	Formic acid
GC	Gas chromatography
GVL	$\gamma$ -valerolactone
HDP	Highest Posterior Density
5-HMF	5-(hydroxymethyl)furfural
INT1	Intermediate 1
LA	Levulinic acid
ODEs	Ordinary differential equation system
OF	objective function
Prot.	Protons
RMF	5-(alcoxymethyl)furfural
ROH	Alcohol
SSR	Sum of squared residuals

## References

- (1) van Zandvoort, I. Towards the Valorization of Humin By-Products : Characterization , Solubilization and Catalysis, Doctoral Thesis, Universiteit Utrecht, 2015.
- (2) Culaba, A. B.; Mayol, A. P.; San Juan, J. L. G.; Vinoya, C. L.; Concepcion, R. S.; Bandala, A. A.; Vicerra, R. R. P.; Ubando, A. T.; Chen, W. H.; Chang, J. S. Smart Sustainable Biorefineries for Lignocellulosic Biomass. *Bioresource Technology*. Elsevier January 1, 2022, p 126215. <https://doi.org/10.1016/j.biortech.2021.126215>.
- (3) Ning, P.; Yang, G.; Hu, L.; Sun, J.; Shi, L.; Zhou, Y.; Wang, Z.; Yang, J. Recent Advances in the Valorization of Plant Biomass. *Biotechnol. Biofuels* 2021 141 **2021**, 14 (1), 1–22. <https://doi.org/10.1186/S13068-021-01949-3>.
- (4) Singhvi, M. S.; Gokhale, D. V. Lignocellulosic Biomass: Hurdles and Challenges in Its Valorization. *Appl. Microbiol. Biotechnol.* 2019 10323 **2019**, 103 (23), 9305–9320. <https://doi.org/10.1007/S00253-019-10212-7>.
- (5) Lu, X.; Lagerquist, L.; Eränen, K.; Hemming, J.; Eklund, P.; Estel, L.; Leveneur, S.; Grénman, H. Reductive Catalytic Depolymerization of Semi-Industrial Wood-Based Lignin. *Ind. Eng. Chem. Res.* **2021**, 60 (47), 16827–16838. [https://doi.org/10.1021/ACS.IECR.1C03154/SUPPL\\_FILE/IE1C03154\\_SI\\_001.PDF](https://doi.org/10.1021/ACS.IECR.1C03154/SUPPL_FILE/IE1C03154_SI_001.PDF).
- (6) Wang, H.; Pu, Y.; Ragauskas, A.; Yang, B. From Lignin to Valuable Products—Strategies, Challenges, and Prospects. *Bioresource Technology*. Elsevier January 1, 2019, pp 449–461. <https://doi.org/10.1016/j.biortech.2018.09.072>.
- (7) Sun, Z.; Fridrich, B.; De Santi, A.; Elangovan, S.; Barta, K. Bright Side of Lignin Depolymerization: Toward New Platform Chemicals. *Chemical Reviews*. American Chemical Society January 24, 2018, pp 614–678. <https://doi.org/10.1021/acs.chemrev.7b00588>.
- (8) Schutyser, W.; Renders, T.; Van Den Bosch, S.; Koelewijn, S. F.; Beckham, G. T.; Sels, B. F. Chemicals from Lignin: An Interplay of Lignocellulose Fractionation, Depolymerisation, and Upgrading. *Chem. Soc. Rev.* **2018**, 47 (3), 852–908. <https://doi.org/10.1039/C7CS00566K>.

- (9) Nzediegwu, E.; Dumont, M. J. Chemo-Catalytic Transformation of Cellulose and Cellulosic-Derived Waste Materials into Platform Chemicals. *Waste and Biomass Valorization*. Springer July 27, 2021, pp 2825–2851. <https://doi.org/10.1007/s12649-020-01179-y>.
- (10) Chen, Y. W.; Lee, H. V. Recent Progress in Homogeneous Lewis Acid Catalysts for the Transformation of Hemicellulose and Cellulose into Valuable Chemicals, Fuels, and Nanocellulose. *Rev. Chem. Eng.* **2020**, 36 (2), 215–235. <https://doi.org/10.1515/revce-2017-0071>.
- (11) Šivec, R.; Grilc, M.; Huš, M.; Likozar, B. Multiscale Modeling of (Hemi)Cellulose Hydrolysis and Cascade Hydrotreatment of 5-Hydroxymethylfurfural, Furfural, and Levulinic Acid. *Ind. Eng. Chem. Res.* **2019**, 58 (35), 16018–16032. <https://doi.org/10.1021/acs.iecr.9b00898>.
- (12) Dusselier, M.; Mascal, M.; Sels, B. F. Top Chemical Opportunities from Carbohydrate Biomass: A Chemist's View of the Biorefinery. *Top. Curr. Chem.* **2014**, 353, 1–40. [https://doi.org/10.1007/128\\_2014\\_544](https://doi.org/10.1007/128_2014_544).
- (13) Delidovich, I.; Leonhard, K.; Palkovits, R. Cellulose and Hemicellulose Valorisation: An Integrated Challenge of Catalysis and Reaction Engineering. *Energy and Environmental Science*. The Royal Society of Chemistry August 13, 2014, pp 2803–2830. <https://doi.org/10.1039/c4ee01067a>.
- (14) Takkellapati, S.; Li, T.; Gonzalez, M. A. An Overview of Biorefinery-Derived Platform Chemicals from a Cellulose and Hemicellulose Biorefinery. *Clean Technol. Environ. Policy* **2018**, 20 (7), 1615–1630. <https://doi.org/10.1007/s10098-018-1568-5>.
- (15) Isikgor, F. H.; Becer, C. R. Lignocellulosic Biomass: A Sustainable Platform for the Production of Bio-Based Chemicals and Polymers. *Polym. Chem.* **2015**, 6 (25), 4497–4559. <https://doi.org/10.1039/C5PY00263J>.
- (16) Kohli, K.; Prajapati, R.; Sharma, B. K. Bio-Based Chemicals from Renewable Biomass for Integrated Biorefineries. *Energies* **2019**, 12 (2), 233. <https://doi.org/10.3390/en12020233>.

- (17) Bozell, J. J.; Patel, M. K.; American Chemical Society. Cellulose and Renewable Materials Division.; American Chemical Society. Meeting (227th : 2004 : Anaheim, C. . Feedstocks for the Future : Renewables for the Production of Chemicals and Materials. **2006**, 378.
- (18) Kapanji, K. K.; Haigh, K. F.; Görgens, J. F. Techno-Economics of Lignocellulose Biorefineries at South African Sugar Mills Using the Biofine Process to Co-Produce Levulinic Acid, Furfural and Electricity along with Gamma Valeractone. *Biomass and Bioenergy* **2021**, *146*, 106008. <https://doi.org/10.1016/j.biombioe.2021.106008>.
- (19) Delgado, J.; Vasquez Salcedo, W. N.; Bronzetti, G.; Casson Moreno, V.; Mignot, M.; Legros, J.; Held, C.; Grénman, H.; Leveneur, S. Kinetic Model Assessment for the Synthesis of  $\gamma$ -Valerolactone from n-Butyl Levulinate and Levulinic Acid Hydrogenation over the Synergy Effect of Dual Catalysts Ru/C and Amberlite IR-120. *Chem. Eng. J.* **2022**, *430*, 133053. <https://doi.org/10.1016/j.cej.2021.133053>.
- (20) Capecchi, S.; Wang, Y.; Delgado, J.; Casson Moreno, V.; Mignot, M.; Grénman, H.; Murzin, D. Y.; Leveneur, S. Bayesian Statistics to Elucidate the Kinetics of  $\gamma$ -Valerolactone from n-Butyl Levulinate Hydrogenation over Ru/C. *Ind. Eng. Chem. Res.* **2021**, *60* (31), 11725–11736. <https://doi.org/10.1021/acs.iecr.1c02107>.
- (21) Casson Moreno, V.; Garbetti, A. L.; Leveneur, S.; Antonioni, G. A Consequences-Based Approach for the Selection of Relevant Accident Scenarios in Emerging Technologies. *Saf. Sci.* **2019**, *112*, 142–151. <https://doi.org/10.1016/j.ssci.2018.10.024>.
- (22) Carnevali, D.; Rigamonti, M. G.; Tabanelli, T.; Patience, G. S.; Cavani, F. Levulinic Acid Upgrade to Succinic Acid with Hydrogen Peroxide. *Appl. Catal. A Gen.* **2018**, *563*, 98–104. <https://doi.org/10.1016/J.APCATA.2018.06.034>.
- (23) Podolean, I.; Kuncser, V.; Gheorghe, N.; MacOvei, D.; Parvulescu, V. I.; Coman, S. M. Ru-Based Magnetic Nanoparticles (MNP) for Succinic Acid Synthesis from Levulinic Acid. *Green Chem.* **2013**, *15* (11), 3077–3082. <https://doi.org/10.1039/C3GC41120F>.
- (24) Adeleye, A. T.; Louis, H.; Akakuru, O. U.; Joseph, I.; Enudi, O. C.; Michael, D. P. A

- Review on the Conversion of Levulinic Acid and Its Esters to Various Useful Chemicals. *AIMS Energy*. AIMS Press 2019, pp 165–185.  
<https://doi.org/10.3934/ENERGY.2019.2.165>.
- (25) Al-Naji, M.; Puértolas, B.; Kumru, B.; Cruz, D.; Bäuml, M.; Schmidt, B. V. K. J.; Tarakina, N. V.; Pérez-Ramírez, J. Sustainable Continuous Flow Valorization of  $\gamma$ -Valerolactone with Trioxane to  $\alpha$ -Methylene- $\gamma$ -Valerolactone over Basic Beta Zeolites. *ChemSusChem* **2019**, *12* (12), 2628–2636. <https://doi.org/10.1002/cssc.201900418>.
- (26) Phanopoulos, A.; White, A. J. P.; Long, N. J.; Miller, P. W. Catalytic Transformation of Levulinic Acid to 2-Methyltetrahydrofuran Using Ruthenium - N-Triphos Complexes. *ACS Catal.* **2015**, *5* (4), 2500–2512.  
[https://doi.org/10.1021/CS502025T/SUPPL\\_FILE/CS502025T\\_SI\\_001.PDF](https://doi.org/10.1021/CS502025T/SUPPL_FILE/CS502025T_SI_001.PDF).
- (27) Licursi, D.; Antonetti, C.; Fulignati, S.; Giannoni, M.; Raspolli Galletti, A. M. Cascade Strategy for the Tunable Catalytic Valorization of Levulinic Acid and  $\gamma$ -Valerolactone to 2-Methyltetrahydrofuran and Alcohols. *Catal.* **2018**, *Vol. 8*, Page 277 **2018**, *8* (7), 277.  
<https://doi.org/10.3390/CATAL8070277>.
- (28) Obregón, I.; Gandarias, I.; Miletic, N.; Ocio, A.; Arias, P. L. One-Pot 2-Methyltetrahydrofuran Production from Levulinic Acid in Green Solvents Using Ni-Cu/Al<sub>2</sub>O<sub>3</sub> Catalysts. *ChemSusChem* **2015**, *8* (20), 3483–3488.  
<https://doi.org/10.1002/CSSC.201500671>.
- (29) Tan-Soetedjo, J. N. M.; Van De Bovenkamp, H. H.; Abdilla, R. M.; Rasrendra, C. B.; Van Ginkel, J.; Heeres, H. J. Experimental and Kinetic Modeling Studies on the Conversion of Sucrose to Levulinic Acid and 5-Hydroxymethylfurfural Using Sulfuric Acid in Water. *Ind. Eng. Chem. Res.* **2017**, *56* (45), 13228–13239.  
[https://doi.org/10.1021/ACS.IECR.7B01611/SUPPL\\_FILE/IE7B01611\\_SI\\_001.PDF](https://doi.org/10.1021/ACS.IECR.7B01611/SUPPL_FILE/IE7B01611_SI_001.PDF).
- (30) Khan, A. S.; Man, Z.; Bustam, M. A.; Nasrullah, A.; Ullah, Z.; Sarwono, A.; Shah, F. U.; Muhammad, N. Efficient Conversion of Lignocellulosic Biomass to Levulinic Acid Using Acidic Ionic Liquids. *Carbohydr. Polym.* **2018**, *181*, 208–214.  
<https://doi.org/10.1016/J.CARBPOL.2017.10.064>.

- (31) Dussan, K.; Girisuta, B.; Haverty, D.; Leahy, J. J.; Hayes, M. H. B. Kinetics of Levulinic Acid and Furfural Production from *Miscanthus × Giganteus*. *Bioresour. Technol.* **2013**, *149*, 216–224. <https://doi.org/10.1016/J.BIORTECH.2013.09.006>.
- (32) Liang, C.; Hu, Y.; Wang, Y.; Wu, L.; Zhang, W. Production of Levulinic Acid from Corn Cob Residue in a Fed-Batch Acid Hydrolysis Process. *Process Biochem.* **2018**, *73*, 124–131. <https://doi.org/10.1016/J.PROCBIO.2018.08.002>.
- (33) Di Menno Di Bucchianico, D.; Wang, Y.; Buvat, J.-C.; Pan, Y.; Casson Moreno, V.; Leveneur, S. Production of Levulinic Acid and Alkyl Levulinates: A Process Insight. *Green Chem.* **2022**, *24*, 614–646. <https://doi.org/10.1039/d1gc02457d>.
- (34) Zhou, L.; Zou, H.; Nan, J.; Wu, L.; Yang, X.; Su, Y.; Lu, T.; Xu, J. Conversion of Carbohydrate Biomass to Methyl Levulinate with  $\text{Al}_2(\text{SO}_4)_3$  as a Simple, Cheap and Efficient Catalyst. *Catal. Commun.* **2014**, *50*, 13–16. <https://doi.org/10.1016/j.catcom.2014.02.021>.
- (35) Saravanamurugan, S.; Riisager, A. Zeolite Catalyzed Transformation of Carbohydrates to Alkyl Levulinates. *ChemCatChem* **2013**, *5* (7), 1754–1757. <https://doi.org/10.1002/cctc.201300006>.
- (36) Hu, X.; Jiang, S.; Wu, L.; Wang, S.; Li, C. Z. One-Pot Conversion of Biomass-Derived Xylose and Furfural into Levulinate Esters via Acid Catalysis. *Chem. Commun.* **2017**, *53* (20), 2938–2941. <https://doi.org/10.1039/C7CC01078H>.
- (37) Wang, Y.; Huang, Y.; Liu, L.; He, L.; Li, T.; Len, C.; Yang, W. Molecular Oxygen-Promoted Synthesis of Methyl Levulinate from 5-Hydroxymethylfurfural. *ACS Sustain. Chem. Eng.* **2020**, *8* (38), 14576–14583. <https://doi.org/10.1021/acssuschemeng.0c05527>.
- (38) Liu, R.; Chen, J.; Huang, X.; Chen, L.; Ma, L.; Li, X. Conversion of Fructose into 5-Hydroxymethylfurfural and Alkyl Levulinates Catalyzed by Sulfonic Acid-Functionalized Carbon Materials. *Green Chem.* **2013**, *15* (10), 2895–2903. <https://doi.org/10.1039/c3gc41139g>.
- (39) Quereshi, S.; Ahmad, E.; Pant, K. K.; Dutta, S. Insights into the Metal Salt Catalyzed

- Ethyl Levulinate Synthesis from Biorenewable Feedstocks. *Catal. Today* **2017**, *291*, 187–194. <https://doi.org/10.1016/j.cattod.2016.12.019>.
- (40) Chithra, P. A.; Darbha, S. Catalytic Conversion of HMF into Ethyl Levulinate – A Biofuel over Hierarchical Zeolites. *Catal. Commun.* **2020**, *140*, 105998. <https://doi.org/10.1016/J.CATCOM.2020.105998>.
- (41) Di Menno Di Bucchianico, D.; Buvat, J.-C.; Mignot, M.; Casson Moreno, V.; Leveneur, S. Role of Solvent the Production of Butyl Levulinate from Fructose. *Fuel* **2022**, *318*, 123703. <https://doi.org/10.1016/j.fuel.2022.123703>.
- (42) An, R.; Xu, G.; Chang, C.; Bai, J.; Fang, S. Efficient One-Pot Synthesis of n-Butyl Levulinate from Carbohydrates Catalyzed by Fe<sub>2</sub>(SO<sub>4</sub>)<sub>3</sub>. *J. Energy Chem.* **2017**, *26* (3), 556–563. <https://doi.org/10.1016/j.jechem.2016.11.015>.
- (43) Kumar, K.; Pathak, S.; Upadhyayula, S. 2nd Generation Biomass Derived Glucose Conversion to 5-Hydroxymethylfurfural and Levulinic Acid Catalyzed by Ionic Liquid and Transition Metal Sulfate: Elucidation of Kinetics and Mechanism. *J. Clean. Prod.* **2020**, *256*, 120292. <https://doi.org/10.1016/j.jclepro.2020.120292>.
- (44) Ariba, H.; Wang, Y.; Devouge-Boyer, C.; Stateva, R. P.; Leveneur, S. Physicochemical Properties for the Reaction Systems: Levulinic Acid, Its Esters, and  $\gamma$ -Valerolactone. *J. Chem. Eng. Data* **2020**, *65* (6), 3008–3020. <https://doi.org/10.1021/acs.jced.9b00965>.
- (45) Konaka, R.; Takahashi, T. A Study of Reaction Rates. Esterification of Formic Acid with Ethanol. *Ind. Eng. Chem.* **2002**, *52* (2), 125–130. <https://doi.org/10.1021/IE50602A027>.
- (46) Bart, H. J.; Reidetschläger, J.; Schatka, K.; Lehmann, A. Kinetics of Esterification of Succinic Anhydride with Methanol by Homogeneous Catalysis. *Int. J. Chem. Kinet.* **1994**, *26* (10), 1013–1021. <https://doi.org/10.1002/kin.550261006>.
- (47) Kokare, M. B.; Ranjani, V.; Mathpati, C. S. Response Surface Optimization, Kinetic Study and Process Design of n-Butyl Levulinate Synthesis. *Chem. Eng. Res. Des.* **2018**, *137*, 577–588. <https://doi.org/10.1016/j.cherd.2018.07.036>.
- (48) Van Putten, R. J.; Van Der Waal, J. C.; De Jong, E.; Rasrendra, C. B.; Heeres, H. J.;

- De Vries, J. G. Hydroxymethylfurfural, a Versatile Platform Chemical Made from Renewable Resources. *Chemical Reviews*. American Chemical Society March 13, 2013, pp 1499–1597. <https://doi.org/10.1021/cr300182k>.
- (49) Russo, V.; Tesser, R.; Rossano, C.; Cogliano, T.; Vitiello, R.; Leveneur, S.; Di Serio, M. Kinetic Study of Amberlite IR120 Catalyzed Acid Esterification of Levulinic Acid with Ethanol: From Batch to Continuous Operation. *Chem. Eng. J.* **2020**, *401*, 126126. <https://doi.org/10.1016/J.CEJ.2020.126126>.
- (50) Sacia, E. R.; Balakrishnan, M.; Bell, A. T. Biomass Conversion to Diesel via the Etherification of Furanyl Alcohols Catalyzed by Amberlyst-15. *J. Catal.* **2014**, *313*, 70–79. <https://doi.org/10.1016/J.JCAT.2014.02.012>.
- (51) Wang, S.; Chen, Y.; Jia, Y.; Xu, G.; Chang, C.; Guo, Q.; Tao, H.; Zou, C.; Li, K. Experimental and Theoretical Studies on Glucose Conversion in Ethanol Solution to 5-Ethoxymethylfurfural and Ethyl Levulinate Catalyzed by a Brønsted Acid. *Phys. Chem. Chem. Phys.* **2021**, *23* (35), 19729–19739. <https://doi.org/10.1039/d1cp02986j>.
- (52) Zheng, X.; Gu, X.; Ren, Y.; Zhi, Z.; Lu, X. Production of 5-Hydroxymethyl Furfural and Levulinic Acid from Lignocellulose in Aqueous Solution and Different Solvents. *Biofuels, Bioprod. Biorefining* **2016**, *10* (6), 917–931. <https://doi.org/10.1002/BBB.1720>.
- (53) Ramírez, E.; Bingué, R.; Fité, C.; Iborra, M.; Tejero, J.; Cunill, F. Assessment of Ion Exchange Resins as Catalysts for the Direct Transformation of Fructose into Butyl Levulinate. *Appl. Catal. A Gen.* **2021**, *612*, 117988. <https://doi.org/10.1016/j.apcata.2021.117988>.
- (54) Zhang, Z. Synthesis of  $\gamma$ -Valerolactone from Carbohydrates and Its Applications. *ChemSusChem* **2016**, *9* (2), 156–171. <https://doi.org/10.1002/CSSC.201501089>.
- (55) Nikbin, N.; Caratzoulas, S.; Vlachos, D. G. A First Principles-Based Microkinetic Model for the Conversion of Fructose to 5-Hydroxymethylfurfural. *ChemCatChem* **2012**, *4* (4), 504–511. <https://doi.org/10.1002/cctc.201100444>.
- (56) Yang, G.; Pidko, E. A.; Hensen, E. J. M. Mechanism of Brønsted Acid-Catalyzed

- Conversion of Carbohydrates. *J. Catal.* **2012**, *295*, 122–132.  
<https://doi.org/10.1016/J.JCAT.2012.08.002>.
- (57) Iborra, M.; Tejero, J.; Fité, C.; Ramírez, E.; Cunill, F. Liquid-Phase Synthesis of Butyl Levulinate with Simultaneous Water Removal Catalyzed by Acid Ion Exchange Resins. *J. Ind. Eng. Chem.* **2019**, *78*, 222–231.  
<https://doi.org/10.1016/J.JIEC.2019.06.011>.
- (58) Musante, R. L.; Grau, R. J.; Baltanás, M. A. Kinetic of Liquid-Phase Reactions Catalyzed by Acidic Resins: The Formation of Peracetic Acid for Vegetable Oil Epoxidation. *Appl. Catal. A Gen.* **2000**, *197* (1), 165–173.  
[https://doi.org/10.1016/S0926-860X\(99\)00547-5](https://doi.org/10.1016/S0926-860X(99)00547-5).
- (59) Leveneur, S.; Wärnå, J.; Eränen, K.; Salmi, T. Green Process Technology for Peroxycarboxylic Acids: Estimation of Kinetic and Dispersion Parameters Aided by RTD Measurements: Green Synthesis of Peroxycarboxylic Acids. *Chem. Eng. Sci.* **2011**, *66* (6), 1038–1050. <https://doi.org/10.1016/J.CES.2010.12.005>.
- (60) Leveneur, S.; De Araujo Filho, C. A.; Estel, L.; Salmi, T. Modeling of a Liquid-Liquid-Solid Heterogeneous Reaction System: Model System and Peroxyvaleric Acid. *Ind. Eng. Chem. Res.* **2012**, *51*, 189–201. <https://doi.org/10.1021/ie2017064>.
- (61) Leveneur, S.; Murzin, D. Y.; Salmi, T.; Mikkola, J.-P.; Kumar, N.; Eränen, K.; Estel, L. Synthesis of Peroxypropionic Acid from Propionic Acid and Hydrogen Peroxide over Heterogeneous Catalysts. *Chem. Eng. J.* **2009**, *147* (2–3).  
<https://doi.org/10.1016/j.cej.2008.11.045>.
- (62) Stewart, W. E.; Caracotsios, M. Athena Visual Studio. <https://athenavisual.com/>  
(accessed May 1, 2022)
- (63) Stewart, W. E.; Caracotsios, M. *Computer-Aided Modeling of Reactive Systems*, Wiley & So.; Wiley & Sons, Ed.; Wiley & Sons: New Jersey, 2008.
- (64) Kopyscinski, J.; Choi, J.; Hill, J. M. Comprehensive Kinetic Study for Pyridine Hydrodenitrogenation on (Ni)WP/SiO<sub>2</sub> Catalysts. *Appl. Catal. A Gen.* **2012**, *445–446*, 50–60. <https://doi.org/10.1016/j.apcata.2012.08.027>.

- (65) Stewart, W. E.; Caracotsios, M.; Sørensen, J. P. Parameter Estimation from Multiresponse Data. *AIChE J.* **1992**, *38* (5), 641–650.  
<https://doi.org/10.1002/aic.690380502>.
- (66) Boekel, M. A. J. S. Van. Statistical Aspects of Kinetic Modeling for Food Science Problems. *J. Food Sci.* **1996**, *61* (3), 477–486. <https://doi.org/10.1111/J.1365-2621.1996.TB13138.X>.
- (67) Caracotsios, M.; Stewart, W. E. Sensitivity Analysis of Initial Value Problems with Mixed Odes and Algebraic Equations. *Comput. Chem. Eng.* **1985**, *9* (4), 359–365.  
[https://doi.org/10.1016/0098-1354\(85\)85014-6](https://doi.org/10.1016/0098-1354(85)85014-6).
- (68) Buzzi-Ferraris, G. Planning of Experiments and Kinetic Analysis. *Catal. Today* **1999**, *52* (2–3), 125–132. [https://doi.org/10.1016/S0920-5861\(99\)00070-X](https://doi.org/10.1016/S0920-5861(99)00070-X).
- (69) McDonald, M. A.; Bromig, L.; Grover, M. A.; Rousseau, R. W.; Bommarius, A. S. Kinetic Model Discrimination of Penicillin G Acylase Thermal Deactivation by Non-Isothermal Continuous Activity Assay. *Chem. Eng. Sci.* **2018**, *187*, 79–86.  
<https://doi.org/10.1016/j.ces.2018.04.046>.
- (70) Toch, K.; Thybaut, J. W.; Marin, G. B. A Systematic Methodology for Kinetic Modeling of Chemical Reactions Applied to N-Hexane Hydroisomerization. *AIChE J.* **2015**, *61* (3), 880–892. <https://doi.org/10.1002/aic.14680>.
- (71) Slotboom, Y.; Bos, M. J.; Pieper, J.; Vrieswijk, V.; Likožar, B.; Kersten, S. R. A.; Brillman, D. W. F. Critical Assessment of Steady-State Kinetic Models for the Synthesis of Methanol over an Industrial Cu/ZnO/Al<sub>2</sub>O<sub>3</sub> Catalyst. *Chem. Eng. J.* **2020**, *389*, 124181. <https://doi.org/10.1016/J.CEJ.2020.124181>.

**Daniele Di Menno Di Bucchianico** obtained his Bachelor's Degree in Chemical and Biochemical Engineering and his Master's Degree in Chemical Process Engineering in 2017 and 2020, respectively, from the University of Bologna, Italy. From the outset, his research activities have focused on biomass and waste valorisation, ranging from the formulation of new materials using waste residues to the kinetic modelling of bio-chemicals production pathways. Then his research career continued with the start of his PhD in 2020 at INSA-Rouen-Normandie (France) in the laboratory of chemical process safety (LSPC) and in joint degree with the University of Bologna. Actually, he is working on the valorisation of lignocellulosic biomass to promising bio-platform molecules, focusing on the optimization and kinetic modelling of biomass-derived sugar monomers and intermediates solvolysis to alkyl levulinates.



**Antonella Cipolla** received her master's degree in Chemical Engineering from the University of Bologna in 2022. During her studies, she conducted a research project at INSA Rouen Normandie with a focus on the production of n-butyl levulinate from the alcoholysis of 5-(hydroxymethyl)furfural.



**Jean-Christophe BUVAT** is Assistant Professor in Chemical Engineering at INSA Rouen in the department “Industrial Risks management”. His main research interests are related to safety of chemical processes. Jean-Christophe Buvat headed the Master's Specialty Department of Industrial Risks from 2011 to 2021. He is Director of the Gaston Berger Center for INSA Rouen Normandie since its creation in April 2021.



**Mélanie Mignot.** Currently assistant professor at the CNRS-COBRA laboratory in INSA Rouen, France, Mélanie Mignot obtained her PhD in analytical chemistry at the University of Rouen in 2016 under the direction of Dr HDR Valérie Peulon Agasse and Pr Pascal Cardinaël. After a temporary teaching and research position at the IUT of Rouen (2016-2017), she completed two postdoctoral fellowships (2017-2019) at KU Leuven University, Belgium, under the supervision of Prof. Deirdre Cabooter, including one through a Marie-Marie FellowshipCurie Individual Fellowship. Her current research areas within the Analysis and Modelling team include the development of new methodologies for the analysis of complex mixtures in ion, liquid and gas chromatography (IC, HPLC, GC), coupled with mass spectrometry (MS). For inorganic compounds such as metals, she is using inductively coupled plasma (ICP) and is particularly interested in the development of chemical speciation methods, including trace analysis, by IC-ICP/MS.



**Valeria Casson Moreno** is Associate Professor in Chemical Engineering. Her main research interests are related to Safety and Sustainability of novel chemical processes and technologies, with particular attention paid to the exploitation of renewable energy sources in the perspective of energy transition.



**Sébastien Leveueur** earned two master's theses: Chemical Engineering & Fine Chemistry (INSA Rouen) and Risk management of chemical hazards (University of Rouen) in 2004. In 2005, he worked for nine months at Åbo Akademi University (Finland) on an industrial project (Kemira company). After this project, he started his doctoral thesis in joint degree between Åbo Akademi University (Finland) and INSA Rouen on "Catalytic synthesis and decomposition of peroxy-carboxylic acids". In 2009, he got his Ph.D. degree with honor from both institutes and the European label. From 2009 to 2010, he continued as a junior researcher at Åbo Akademi University and focused his research on kinetic modeling in the continuous reactor.

He was appointed Assistant-Professor at INSA Rouen in 2010 in the department "Risk management." In 2015, he defended his Habilitation (University of Rouen) and became Associate-Professor. In 2015, he was also appointed ***Docent in chemical process technology, especially new concepts chemical in reaction engineering, modelling of chemical reactors and safety aspects*** at Åbo Akademi University. This position was renewed for life in 2020.

His group aims to understand the reactivity of complex chemical systems: develop robust and reliable kinetic models in different thermal modes. They use different calorimeters (RC1, C80, ARSST, etc), process intensification systems (micro-reactor, microwave irradiation) and statistical methods (Bayesian inferences, cross-validation, etc).

